



# Reconstructing the advance and retreat dynamics of the central sector of the last Cordilleran Ice Sheet

Helen E. Dulfer<sup>a,\*</sup>, Martin Margold<sup>a</sup>, Christopher M. Darvill<sup>b</sup>, Arjen P. Stroeven<sup>c,d</sup>

<sup>a</sup> Department of Physical Geography and Geoecology, Faculty of Science, Charles University in Prague, Albertov 6, 12800, Praha, Czech Republic

<sup>b</sup> Department of Geography, The University of Manchester, Arthur Lewis Building, Oxford Road, Manchester, M13 9PL, UK

<sup>c</sup> Geomorphology and Glaciology, Department of Physical Geography, Stockholm University, 106 91, Stockholm, Sweden

<sup>d</sup> Bolin Centre for Climate Research, Stockholm University, 106 91, Stockholm, Sweden

## ARTICLE INFO

### Article history:

Received 22 November 2021

Received in revised form

5 March 2022

Accepted 19 March 2022

Available online xxx

Handling Editor: C. Hillaire-Marcel

### Keywords:

Pleistocene

Paleoglaciology

North America

Glacial geomorphology

## ABSTRACT

The advance of the Cordilleran Ice Sheet (CIS) towards its Last Glacial Maximum (LGM) configuration and its subsequent retreat remain poorly understood. We use the glacial landform record to determine ice dynamics for the central sector of the CIS in northern British Columbia, Canada, beneath the LGM ice divide. We classify seventy ice-flow indicator flowsets based on morphology, elevation, orientation and cross-cutting relationships into one of three stages, whereby stage 1 is oldest and stage 3 youngest. Combined with ice-contact geomorphology, our reconstruction highlights complex changes in ice flow over time as a result of ice divide migrations through the LGM and deglacial phases. The orientation and distribution of landforms indicates active post-LGM ice retreat westward through the Cassiar and Omineca mountains. We map the regional distribution of independent mountain glaciers, ice caps, and ice fields that regrew during a cooling event in the Late Glacial and show that some of these readvance glaciers were subsequently overrun by advancing outlet glaciers of the CIS. We use the cross-cutting relationship between readvance glaciers and CIS outlet glaciers and available chronological data to reconstruct the eastern CIS margin during the Late Glacial for the first time.

© 2022 The Authors. Published by Elsevier Ltd. This is an open access article under the CC BY license (<http://creativecommons.org/licenses/by/4.0/>).

## 1. Introduction

The Cordilleran Ice Sheet (CIS) formed part of the North American Ice Sheet Complex at the Last Glacial Maximum (LGM; Fig. 1) and contained an ice volume similar to that of the present-day Greenland Ice Sheet (equivalent to 7–9 m of sea-level change; Seguinot et al., 2016). Numerical modelling of the CIS during the last glacial cycle (~120 ka) indicates the central sector of the ice sheet in the mountains of northern British Columbia was a nucleation center for ice sheet growth in both Marine Isotope Stage (MIS) 4 and MIS 2 (Fig. 2; Seguinot et al., 2016). However, few empirical constraints are available on the nature of ice build-up and retreat in this central region of the ice sheet (Clague and Ward, 2011).

Field evidence relating to CIS build-up is fragmentary and consists of (1) sparse, poorly-preserved, and scattered traces of pre-LGM ice flow indicators (Stumpf et al., 2000; Kleman et al., 2010); (2) glaciolacustrine sediments relating to advance-phase glacial

lakes, such as Glacial Lake Stikine (Ryder and Maynard, 1991; Spooner and Osborn, 2000); and (3) overridden cirques (Ryder and Maynard, 1991). A well-established conceptual model proposes ice nucleated on the high mountain peaks of British Columbia (e.g. in the Coast and Skeena mountains), forming ice fields and ice caps that expanded as the climate cooled further, eventually coalescing to form an ice sheet (Fig. 2d–f; Flint, 1943; Davis and Mathews, 1944; Clague, 1980; Fulton, 1991; Ryder and Maynard, 1991; Clague and Ward, 2011). This is supported by the numerical modelling of Seguinot et al. (2016).

Within this conceptual model, ice flow direction would have shifted through time as separate ice dispersal centers coalesced, and ice divides migrated from ice build-up to the ice sheet maximum and then deglaciation phases. Cross-cutting striae provide evidence of ice flow direction progression, including complete ice flow reversals at some locations (Watson and Mathews, 1944; Ryder and Maynard, 1991; Stumpf et al., 2000). Although maps of CIS flow indicators have been produced (Kleman et al., 2010; Shaw et al., 2010; Arnold et al., 2016), there is a lack of information about when they were active in time and space, and therefore, precise changes in ice flow direction and location of ice divides in

\* Corresponding author.

E-mail address: [dulferh@natur.cuni.cz](mailto:dulferh@natur.cuni.cz) (H.E. Dulfer).

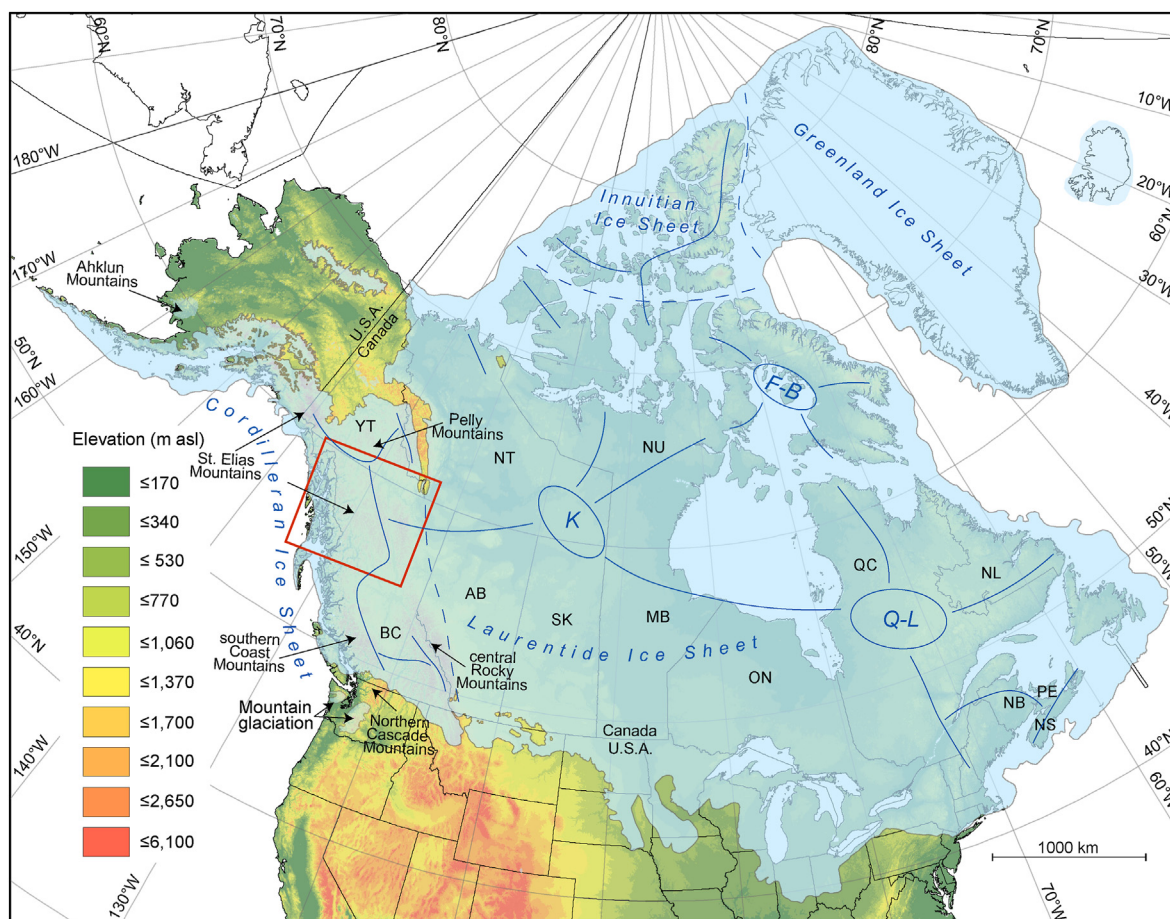


**Fig. 1.** The North American Ice Sheet Complex at 22.1 cal ka BP based on Dalton et al. (2020), Clague and Ward (2011), Menounos et al. (2017) and Margold et al. (2018). Approximate positions of ice divides and ice domes are shown by solid blue lines (K = Keewatin dome, Q-L = Québec-Labrador dome, F-B = Foxe Baffin dome) and blue dashed lines show the location of the suture zones between the ice sheets. The extent of the Greenland and Iceland ice sheets is also shown. It should be noted that in the south, mountain glaciation is shown in the Olympic and Cascade mountains but the local LGM occurred later than 22.1 cal ka BP, and therefore, the maximum southern ice extent is not shown here. Our study area in northern British Columbia is shown by the red box. The provinces of Canada are labelled with abbreviations and the mountain ranges that contain evidence of Late Glacial readvances are also labelled. (For interpretation of the references to colour in this figure legend, the reader is referred to the Web version of this article.)

northern British Columbia remain unclear.

The lack of recessional moraines and presence of kettle and kame topography associated with CIS deglaciation in British Columbia has led to a long-held conceptual model of large-scale downwasting and stagnation of ice in valleys (Davis and Mathews, 1944; Fulton, 1991; Lakeman et al., 2008a; Clague and Ward, 2011; Menounos et al., 2017). However, the extent of vertical ice sheet thinning remains poorly constrained (Margold et al., 2014; Darvill et al., in press; Menounos et al., 2017; Dulfer et al., 2021), and active frontal retreat of outlet glaciers around the periphery of the ice sheet is now well established (Margold et al., 2013a,b; Perkins and Brennand, 2015; Brennand and Perkins, 2017).

CIS configuration during the Late Glacial Bølling-Allerød interstadial (14.6–12.9 ka) and Younger Dryas stadial (YD; 12.9 to 11.7 ka; Rasmussen et al., 2014) is particularly enigmatic. Recent Glacial Isostatic Adjustment (GIA) models suggest these rapid climate oscillations had a dramatic effect on CIS thickness, with abrupt Bølling-Allerød warming causing significant ice sheet thinning and ~50% mass loss (Peltier et al., 2015; Lambeck et al., 2017). Alpine glaciers subsequently expanded in the former central sector of the CIS (Ryder and Maynard, 1991; Lakeman et al., 2008a; Menounos et al., 2017). Nonetheless, CIS configuration during the Late Glacial remains poorly known, particularly as radiocarbon-based

reconstructions do not adequately capture changing ice patterns through mountainous terrain in northern British Columbia (Fig. 3; Dyke, 2004; Dalton et al., 2020).

Here, we use a glacial landform inventory for the central sector of the CIS (Dulfer and Margold, 2021) to resolve the ice dynamics in northern British Columbia. We use flowset classification and interpretation to unravel complex ice flow directions and document ice divide migration between advance, maximum and deglacial phases (Kleman and Borgström, 1996; Kleman et al., 1997, 2006; Greenwood and Clark, 2009). We then use the distribution of ice-marginal moraines, lateral and submarginal meltwater channels, kame terraces, and ice contact deltas to determine the relative deglaciation pattern (Kleman et al., 1997; Greenwood et al., 2007; Chandler et al., 2018) and establish the ice sheet configuration during the Late Glacial period for the first time.

## 2. Methods

Our interpretation of ice dynamics in northern British Columbia is based on the integration of geomorphological data with published geochronological data (primarily cosmogenic nuclide and radiocarbon ages).

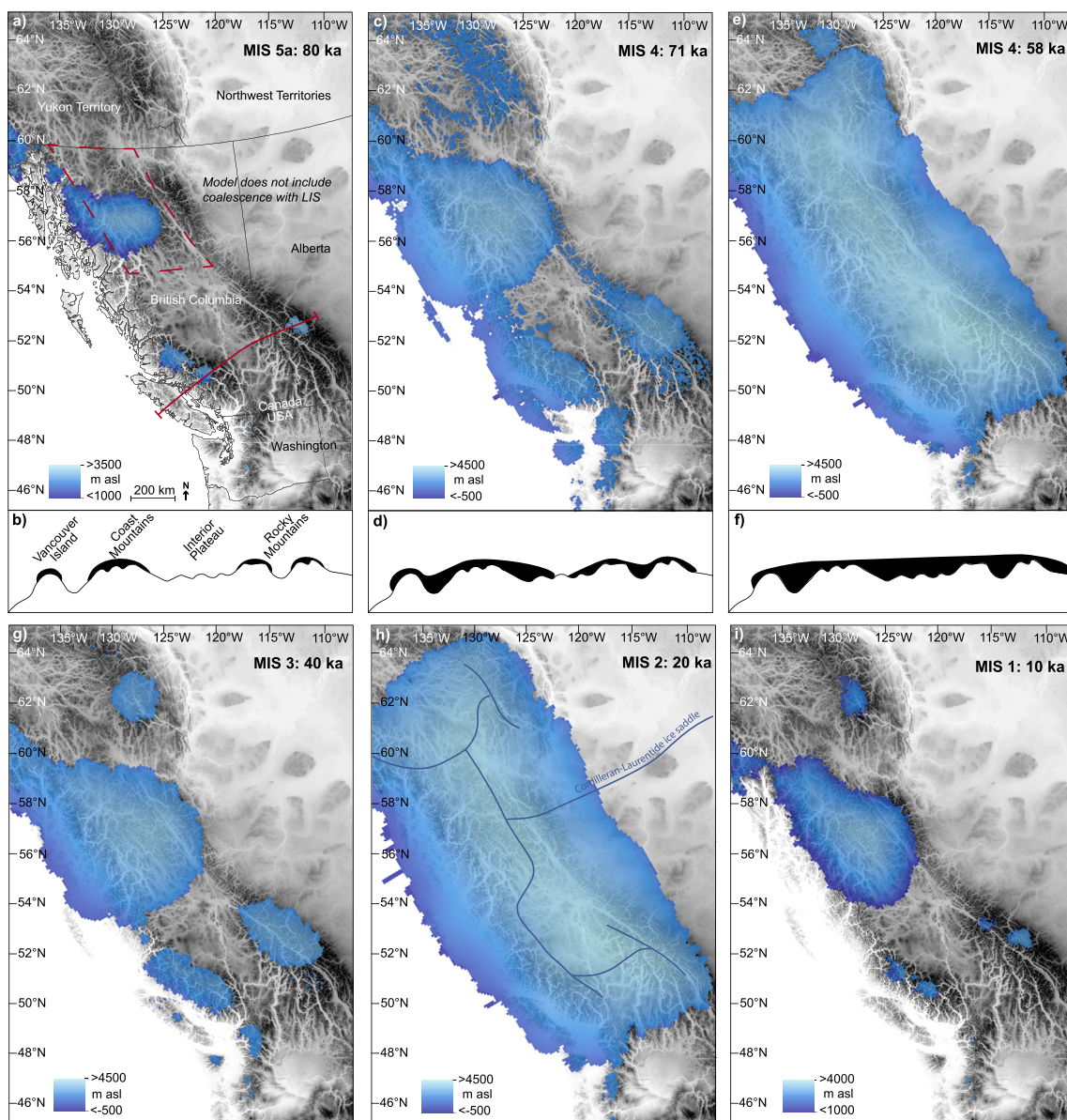


**Fig. 2.** Extent and height (ice thickness plus topography) of the CIS at six different time slices through the last glacial cycle from the numerical model of Seguinot et al. (2016) and Seguinot (2020) using GRIP ice core temperature forcing and cross-profiles showing the conceptual model of ice advance from Fulton (1991). (a) Modelled ice surface at 80 ka showing ice caps nucleating on high mountain peaks, as predicted by the Fulton (1991) conceptual model drawn along the red line (b). The red dashed box shows the area mapped by Dulfer and Margold (2021). (c) Modelled ice surface at 71 ka and accompanying conceptual model (d) showing ice expanding and starting to coalesce at the start of MIS 4. (e) Maximum modelled ice surface during MIS 4 and accompanying conceptual model (f). (g) Modelled ice surface at 40 ka predicting that the central CIS persisted during MIS 3. (h) Modelled ice surface at the LGM (20 ka) with approximate ice divides shown from Clague and Ward (2011), Menounos et al. (2017), and Margold et al. (2019). Note that CIS-Laurentide Ice Sheet coalescence is not accounted for by Seguinot et al. (2016). (i) Modelled ice surface during deglaciation (10 ka). (For interpretation of the references to colour in this figure legend, the reader is referred to the Web version of this article.)

## 2.1. Glacial inversion

The map of Dulfer and Margold (2021) spans 55–60°N and 122.6–135.5°W (Fig. 3) and consists of seven glacial landform categories: ice-flow parallel lineations, moraines (CIS outlet glacier moraines, Late Glacial moraines, and those of unknown origin), meltwater channels (lateral and submarginal, subglacial, proglacial, and origin unknown), kame terraces, eskers (single ridges and esker complexes), perched deltas, and subglacial ribs. Here, we invert the spatial distribution and characteristics of glacial

landforms—including cross-cutting relationships—to decipher the configuration of the ice sheet over time (Kleman and Borgström, 1996; Kleman et al., 2006; Greenwood et al., 2007).

### 2.1.1. Glacial flowsets

Ice flow across the central sector of the CIS has been documented by numerous researchers, with Kleman et al. (2010) and Shaw et al. (2010) producing generalized ice flow maps and Arnold et al. (2016) compiling a database with all published ice flow parallel lineations in British Columbia and the Yukon Territory. Here

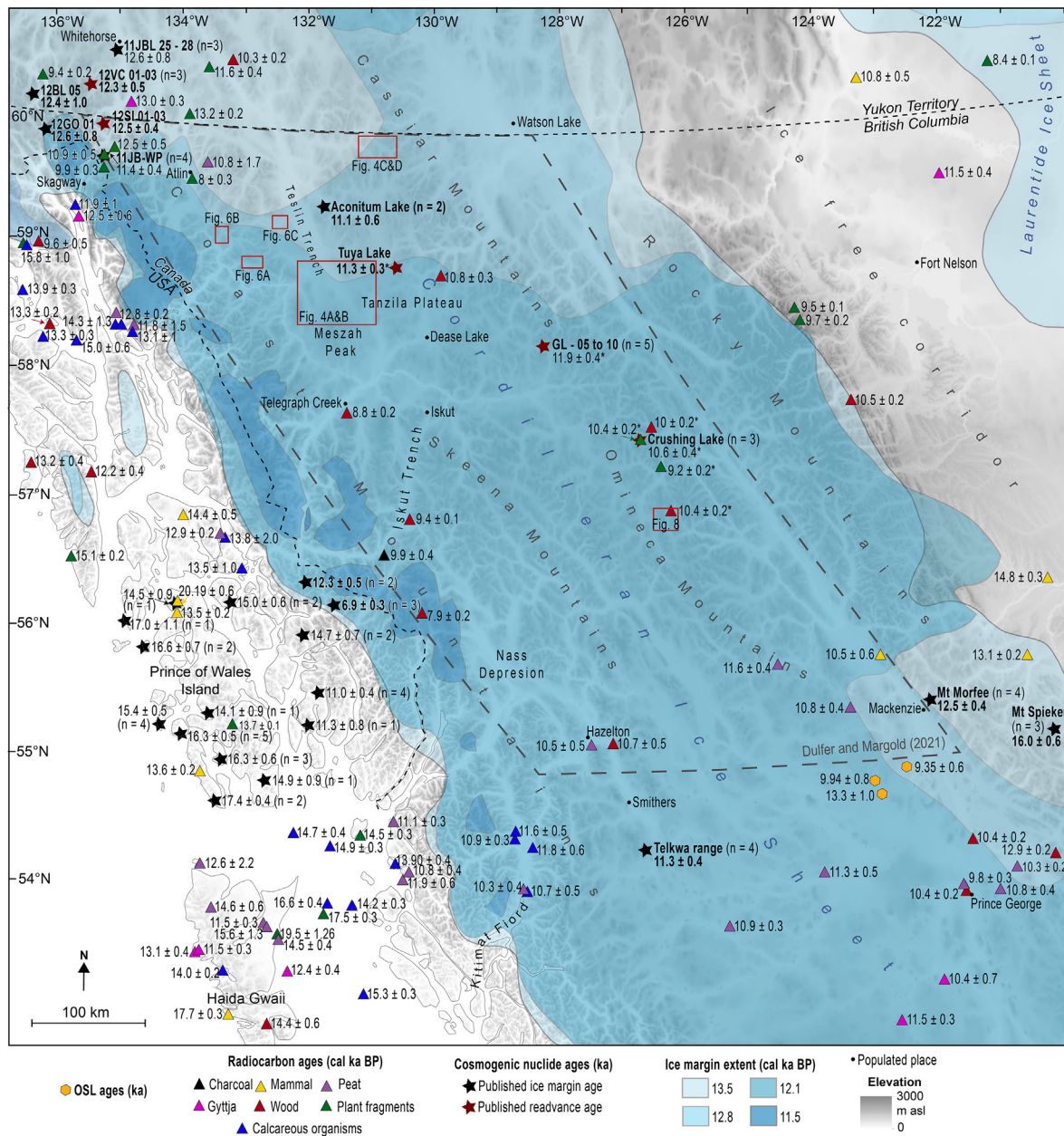


**Fig. 3.** Map showing our current understanding of ice retreat for the central sector of the Cordilleran Ice Sheet (CIS). Blue shading shows the <sup>14</sup>C-based ice retreat chronology from Dalton et al. (2020) and Dyke (2004) for the Late Glacial period (between 13.5 and 11.5 cal ka BP). Nunataks are not shown. Triangles show calibrated radiocarbon ages in cal ka BP (reported at the mid-point of all age ranges at 2-sigma, ± half the total age range) and are minimum ages for deglaciation (see data file S3). Stars show selected <sup>10</sup>Be cosmogenic nuclide exposure ages from Margold et al. (2014), Menounos et al. (2017), Lesnek et al. (2018, 2020) and Dulfer et al. (2021). All ages have been recalculated using the exage exposure age calculator of Heyman (2021; version 201912), which corrects for glacioisostatic rebound. Ages in bold have also been corrected for snow cover. All ages are weighted means with a weighted 1σ external error in thousands of years (ka) based on the number of samples (n). Ages that are marked with asterisks are inferred to relate to a Late Glacial readvance of alpine glaciers, rather than the CIS retreat as described in Lakeman et al. (2008b) and Menounos et al. (2017). Orange hexagons show optically stimulated luminescence (OSL) ages from Sacco et al. (2017). Extent of the Dulfer and Margold (2021) glacial geomorphological map is shown by the grey dashed box. The location of Figs. 4, 6 and 8 are indicated by red boxes. (For interpretation of the references to colour in this figure legend, the reader is referred to the Web version of this article.)

we use the ice flow parallel lineations mapped by Dulfer and Margold (2021) to determine ice flow variation through time. We followed an established approach of grouping coherent patterns of glacial lineations into discrete flowsets (Fig. 4a and b) and use cross-cutting relationships to assign a relative age to the flowsets based on the principle of superposition (Kleman and Borgström, 1996; Kleman et al., 1997; Greenwood and Clark, 2009; Stokes et al., 2015).

However, the highly variable topography of the central sector of the CIS means that many of the discrete flowsets do not overlap.

Therefore, we also use the morphology, location, flow direction and association with other glacial landforms to assist with the classification (criteria outlined in Table 1). This resulted in each flowset being classified into one of three stages, whereby stage 1 is oldest and stage 3 youngest. Flowsets are classified as stage 1 when they have a weathered or degraded appearance and they are often cross-cut by younger flowsets. Where flowsets are produced by ice flow that is independent of topography they are classified at stage 2, and it follows, that stage 2 flowsets are mostly preserved on the high mountain peaks and ridges. A number of criteria is used to classify

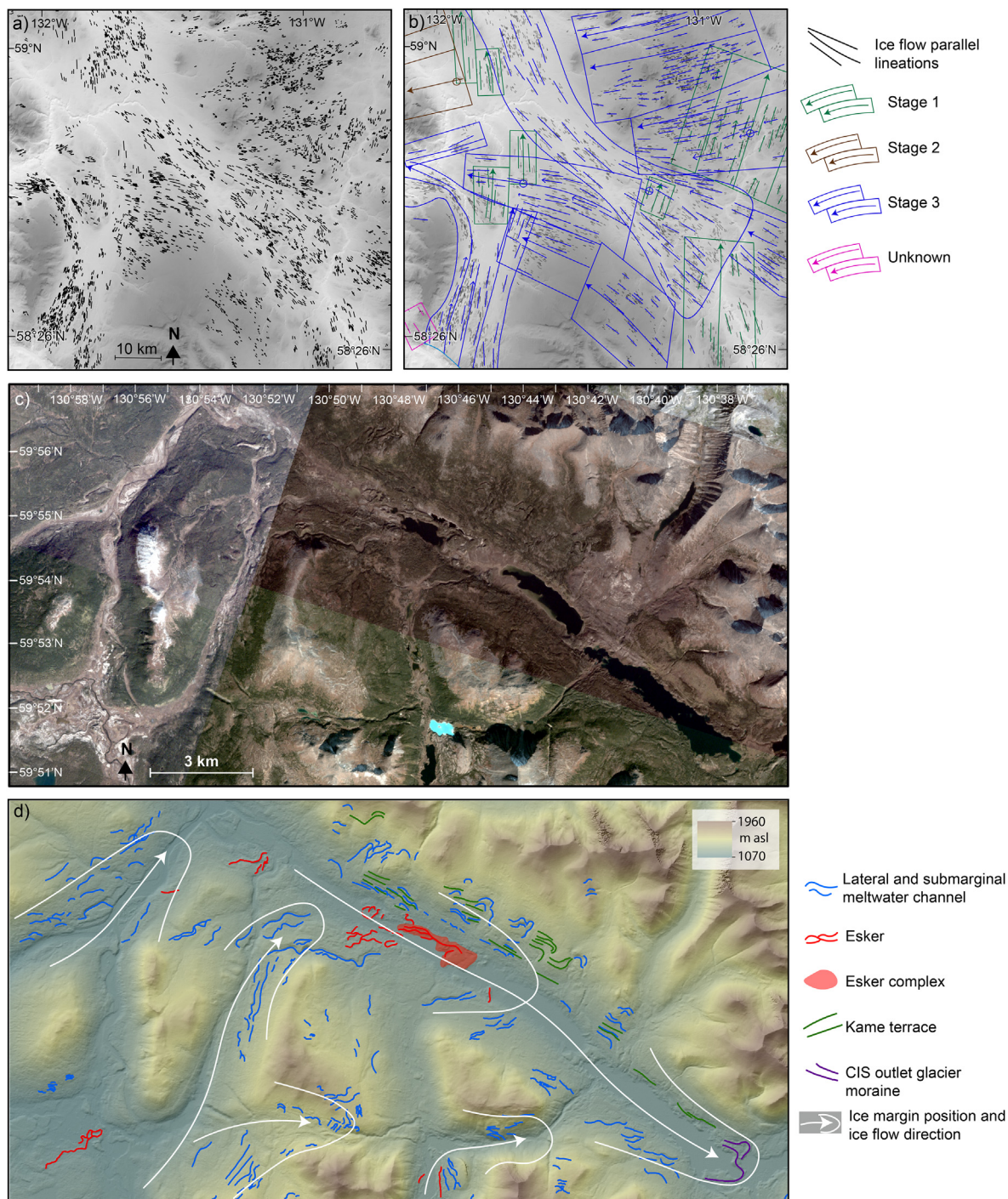


**Fig. 4.** Examples of how the glacial landform record is used to determine ice advance and retreat patterns. (a) Ice flow parallel lineations from Dulfer and Margold (2021) and (b) inferred lineation flowsets. Arrows show ice flow direction and coloured circles show the youngest flowset where cross-cutting relationships occur. (c) High-resolution satellite imagery (Planet Team, 2017) and (d) associated Tandem X-derived hillshade imagery (German Aerospace Center, 2018) with glacial geomorphology from Dulfer and Margold (2021) and interpreted ice flow directions and key marginal positions. Here the glacial meltwater record is key for delineating former ice marginal positions, with many of the ice margins being mapped based on the orientation and direction of successive lateral and submarginal meltwater channels that dip into the valleys.

flowsets into stage 3 including well preserved, highly parallel lineations that are produced by ice flow that is deflected or channelled by topography. Where the relative position of a flowset could not be determined due to a lack of information it was classified as unknown.

### 2.1.2. Deglacial dynamics

We use the distribution of CIS outlet glacier moraines and glacial meltwater landforms (e.g. lateral and submarginal meltwater channels, kame terraces, eskers, and perched deltas) to delineate CIS ice marginal positions during deglaciation (Fig. 4c and d). A brief description and characterization of these landforms is given below.

**Table 1**

Diagnostic criteria for assigning a relative age to the flowsets, whereby stage 1 flowsets are oldest and stage 3 youngest.

Stage 1	- Degraded ice flow parallel lineations. - Usually overprinted by younger flowsets.
Stage 2	- Orientation of the lineations disregards the topography. - Lineations located on high mountain peaks.
Stage 3	- Well-preserved lineations - High parallel conformity. - Lineations can be aligned with ice-marginal landforms such as lateral meltwater channels and eskers. - Lineations can occur both within valleys and on the adjacent mountain peaks. - Lineations deflected by topography.

CIS outlet glacier moraines: sharp-crested, straight or arcuate-shaped ridges of sediment that were deposited along active ice margins. These moraines are inferred to relate to CIS outlet glacier marginal positions during deglaciation based on their morphology, orientation and location proximal to other ice marginal landforms, such as kame terraces and lateral and submarginal meltwater channels (Dulfer and Margold, 2021).

Lateral and submarginal meltwater channels: channels formed by water flowing along the ice margin, and consequently, delineating the glacier margin at the time of formation. Sequences of parallel lateral meltwater channels, with many channels bending down into the valleys, can be used to determine ice surface lowering and marginal retreat through time (Fig. 4d; Mannerfelt, 1949; Greenwood et al., 2007, 2016; Margold et al., 2013b).

Kame terraces: flat-to gently-sloping accumulations of glaciofluvial sediment deposited along lateral glacier margins, often in association with lateral and submarginal meltwater channels. Kame terraces record ice margin position and approximate ice surface elevation at the time of deposition (Brown, 1931; Borsellino et al., 2017; Shulmeister et al., 2018).

Perched deltas: flat-topped accumulations of sediment with steeply-dipping fronts formed by the deposition of sediment into ice-marginal lakes. Perched deltas mark former glacial-lake levels that can be used to determine the ice margin position at the time of formation (Mannerfelt, 1945; Plouffe, 2000; Perkins and Brennand, 2015; Stroeven et al., 2016).

Eskers: ridges of glaciofluvial sediment deposited by meltwater flowing through, beneath, or above ice. Eskers are assumed to form time-transgressively, close to the ice margin and are aligned roughly normal to the margin (Hebrand and Åmark, 1989; Brennand, 2000; Livingstone et al., 2015; Stroeven et al., 2016; Hewitt and Creyts, 2019).

The glacial landform record of the CIS is dominated by glacial meltwater landforms rather than recessional moraines. Dulfer and Margold (2021) record just 97 CIS outlet glacier moraine ridges compared to ~18,000 lateral and submarginal meltwater channels. Consequently, our reconstruction of ice retreat in northern British Columbia relies heavily on glacial meltwater landforms, which constitute a suite of diachronous features documenting successive stages of deglaciation as shown in Fig. 4c and d.

## 2.2. Geochronological dataset

We have compiled datasets of both radiocarbon and cosmogenic nuclide dates from the literature across northern British Columbia, southeastern Alaska and southern Yukon Territory (dataset extent shown in Fig. 3, see supplementary data files S1 and S3). Both datasets have been recalibrated and the details of these calibrations are outlined below.

### 2.2.1. $^{10}\text{Be}$ cosmogenic nuclide ages

Cosmogenic nuclide data offer a direct age on the time of emplacement of boulders and other lithic material by the ice sheet.

All previously published  $^{10}\text{Be}$  ages presented in this paper have been recalculated with the expage exposure age calculator version 201912 (Heyman, 2021), which uses code based on the online calculator of Balco et al. (2008; version 2.0), with the 'primary' calibration set of Borchers et al. (2016) and the CRONUS LSD production rate scaling model (Lifton et al., 2014). Individual ages are reported with external errors ( $1\sigma$ ). Where multiple ages are available for a particular site, a weighted mean age with a weighted mean external error has been calculated (excluding outliers; supplementary data file S1).

GIA-corrected ages were calculated with the exposure age calculator of Heyman (2021), which uses the published relative sea level change ( $\Delta\text{RSL}$ ) data from Lambeck et al. (2017;  $0.25^\circ \times 0.25^\circ$  resolution and 500 year intervals from 25 ka to present) by interpolating the elevation of each sample over time to the cosmogenic nuclide production. This allows the changes in production rate due to GIA to be modified continuously back in time. The GIA correction is most significant at the Mt. Spieker field site in the northern Rocky Mountains where the ages are up to 7% older after the GIA correction is applied (Dulfer et al., 2021). At all other sites the GIA correction alters the age by less than 3.5% (see supplementary data file S1).

We apply a snow shielding correction to exposure ages where average contemporary snow depth per month exceeds the height of the boulder or bedrock samples. Consequently, the majority of ages located in the interior of British Columbia have been corrected for snow cover (with the exception of GL-5 to -10 where boulder heights exceed snow depth for the majority of the year, and Crushing Lake where boulder heights are unknown; Menounos et al., 2017). Coastal sites do not receive enough modern snow cover to justify corrections to their exposure ages (see Fig. 3 and supplementary data file S1).

Where applicable, a snow shielding factor was calculated at each boulder for each month of the year. Monthly snow depth and density data were obtained from nearby manual weather stations (Vionnet et al., 2021) and used to calculate the snow shielding factor according to the exponential attenuation equation for snow shielding presented in Gosse and Phillips (2001). The results were then averaged to give an annual snow shielding factor for each sample. For the purposes of estimating the effect of snow cover, we assume snow shielding remained constant throughout the exposure history. Combined, the snow cover and GIA corrections can increase sample ages by up to 16.4% (RM18-08 from Mt. Spieker), but, the average increase in age is 7% (see supplementary data file S1).

### 2.2.2. Radiocarbon ages

Radiocarbon methods are frequently used to date organic material that emerged in newly deglaciated landscapes, therefore, these data offer a minimum constraint on the ice margin. Radiocarbon ages used in this study are from the database of Dalton et al. (2020), recalibrated using CALIB Rev. 8.1.0 (Stuiver and Reimer, 1993), with the IntCal20 calibration curve (Reimer et al., 2020)

and marine curve (Heaton et al., 2020). Ages are reported at the mid-point of all age ranges at 2-sigma, with the error reported as  $\pm$  half the total age range.

### 3. Results

#### 3.1. Glacial flowsets

We mapped seventy flowsets over the central sector of the CIS (Fig. 5). Variations in flowset orientation and flowset cross-cutting relationships indicate ice flow direction shifted numerous times through the last glacial cycle. Here we briefly describe the characteristics of each flowset category. A full description and comparison with the previous mapping of Kleman et al. (2010), Shaw et al. (2010), and Arnold et al. (2016) are provided in supplementary data file S2.

**Stage 1:** Small, discrete flowsets primarily made up of drumlins and crag-and-tails (maximum area of 30 km<sup>2</sup>). Lineations within these flowsets are weathered and the majority are overprinted by younger flowsets (Fig. 6a). Directional ice flow indicators were identified on flowsets (Fs)35, 38, 56, 57 and 58, indicating that they were produced by northward-flowing ice.

**Stage 2:** Comprised of both small discrete flowsets and large, regionally-extensive flowsets (e.g. Fs15, 50 and 55). Most of the stage 2 flowsets are made of up of lineations that are eroded into

the bedrock on the high mountain peaks (between 1500 and 1850 m asl; Fig. 6c). The ice flow direction is variable but the overall pattern shows eastward flow on the eastern side of the map and westward flow on the western side.

**Stage 3:** This phase consists of the largest number of flowsets. Consequently, their morphology is highly variable and the ice-flow parallel lineations occur over a wide range of elevations (800–1900 m asl). Nonetheless, all the stage 3 flowsets contain well-preserved ice-flow parallel lineations that show a high parallel conformity (Fig. 6a and b) and almost half of these flowsets are aligned with deglacial landforms.

Some stage 3 flowsets are large and regionally extensive (e.g. Fs4, 5, 13, and 60; maximum area of 200 km<sup>2</sup>). Thus, it is possible that the ice-flow parallel lineations within these flowsets formed at different times (time transgressively). We group these lineations together into flowsets because it is impossible to differentiate different phases of ice flow. This method is supported by Kleman et al. (2010) who map numerous large flow systems across the CIS. For example, Fs4 forms part of the Prince George flow system mapped by Kleman et al. (2010) and shows the ice flow direction evolved from westerly through to southerly ice flow. Additionally, the red stars in Fig. 5 show two locations where stage 3 flowsets with different flow directions are juxtaposed: (1) northward flowing Fs23 and 65 and southward flowing Fs21; and (2) northeast flowing Fs51 and southward flowing Fs53.

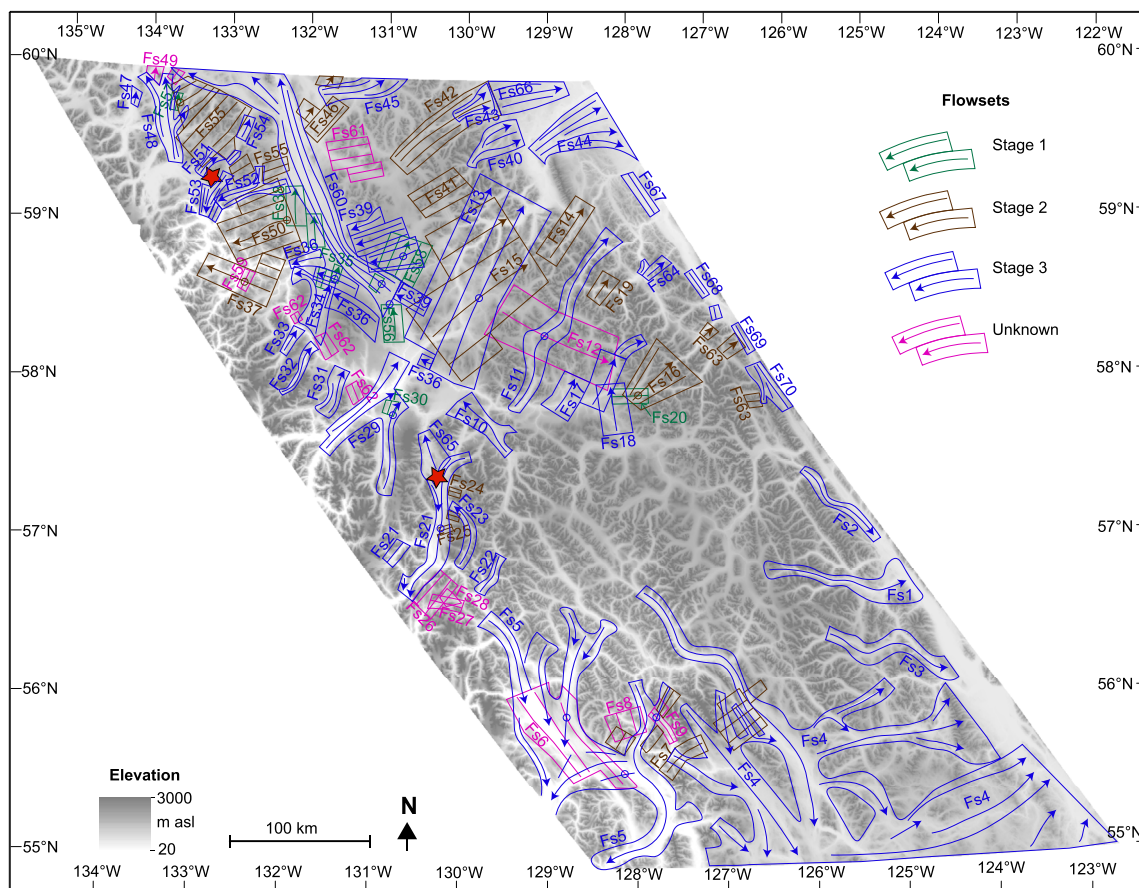


**Fig. 5.** Flowset map of the central sector of the Cordilleran Ice Sheet. Each flowset has been assigned a number corresponding to additional information in supplementary data file S2. The flowsets have been categorized into stages 1–3 based on their morphology, location, flow direction, association with other glacial landforms and overprinting relationships (see Table 1). Where the flowset does not fit into one of the stages it has been classified as an unknown flowset. The arrows show the ice flow direction where it could be discerned from the morphology of the glacial lineations. Red stars show the location of ice flow reversals during stage 3. It should be noted that some flowsets consist of several elements that display the same morphology but are spatially separate. (For interpretation of the references to colour in this figure legend, the reader is referred to the Web version of this article.)

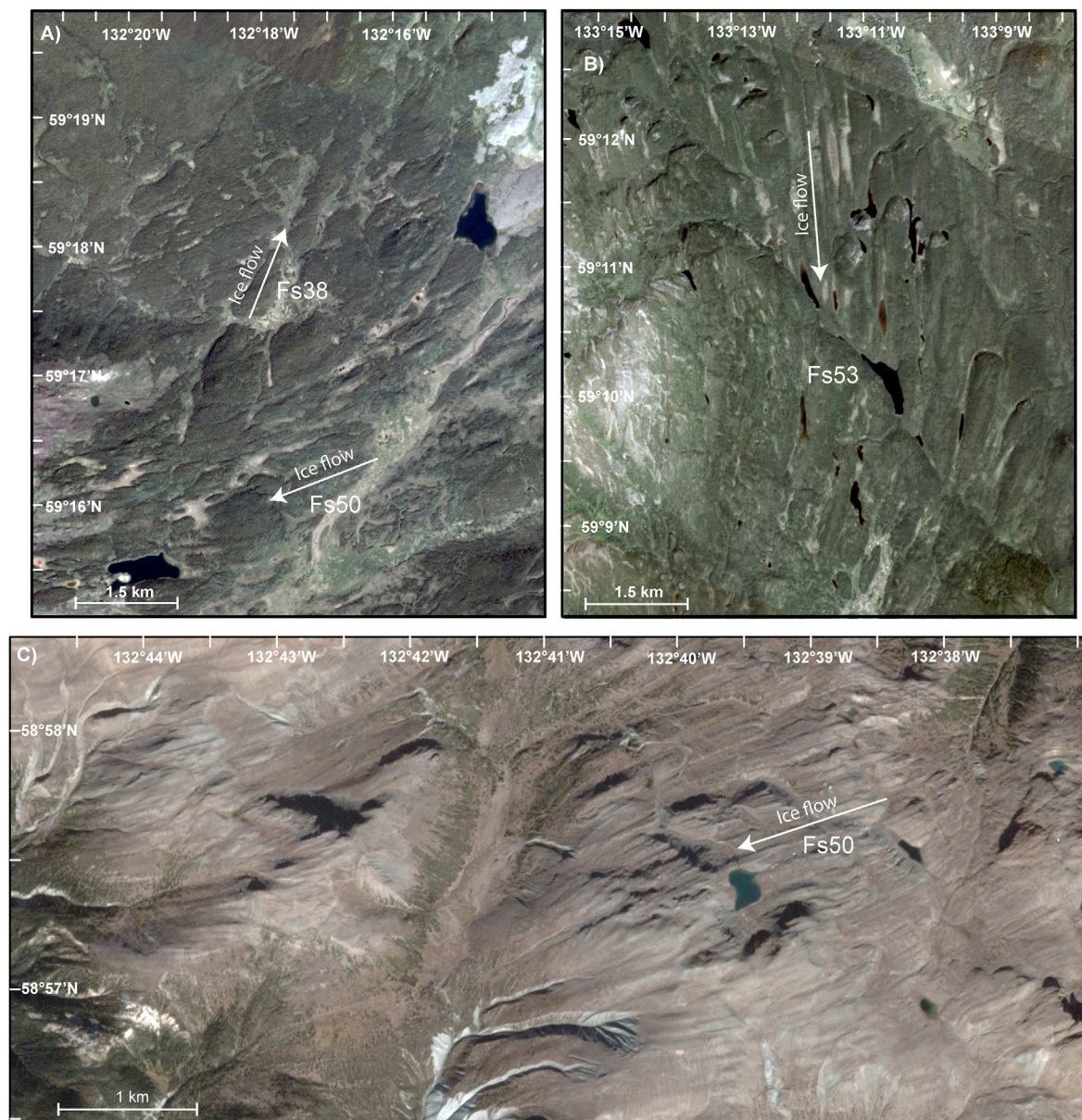


**Fig. 6.** High resolution Planet Team (2017) satellite imagery showing examples of flowsets from stages 1–3. (a) Example of a stage 1 flowset (Fs38) with ice flow to the north that is overprinted by a stage 3 flowset (Fs50) with ice flow to the west. (b) Drumlins and crag-and-tails that form part of a stage 3 flowset (Fs53) and (c) Streamlined bedrock that forms part of a stage 2 flowset (Fs50).

**Unknown flowsets:** Occur where the relative position of a flowset could not be discerned from their morphology, orientation or cross-cutting relationships. Two noteworthy examples are Fs12 and 6. Fs12 consists of streamlined bedrock on high mountain peaks (up to 1800 m asl), offset by 90° to surrounding flowsets. Cross-cutting lineations show Fs12 was created before Fs11. The streamlined landforms within Fs12 have not previously been recognised, probably because bedrock structures in this area have the same orientation. However, the high-resolution satellite imagery used in this study allowed us to determine the bedrock structures have been glacially eroded. Fs6 is primarily composed of heavily-eroded bedrock. Cross-cutting lineations indicate Fs6 is older than Fs5 (stage 3) but we are unable to classify this flowset further, although Kleman et al. (2010) draw Fs5 and 6 as one Late Wisconsinan flow system.

**Comparison to previous work:** Our flowsets were mapped

independently of the information available in the literature, and therefore, within [supplementary data file S2](#), we have marked whether our flowsets have been previously recognised. It should be noted that as the other authors did not classify their lineations into flowsets, we compare our flowsets with their mapped lineations or ice flow indicators. Our mapping based on Dulfer and Margold (2021) yields similar results to the detailed compilation of Arnold et al. (2016), but, unlike that study, we classify our lineations into flowsets and assign them relative ages to allow much greater insight into central CIS evolution over the last glaciation. The ice flow map of Shaw et al. (2010) captures 30% of the flowsets mapped in this study.

Approximately 70% of our flowsets match those of Kleman et al. (2010). In particular, many of our stage 3 flowsets were also recorded by Kleman et al. (2010). However, there are significant differences between our flowset classifications, notably around

Meszah Peak and Tanzila Plateau (see Fig. 3 for location). At these locations, Kleman et al. (2010) classified the ice-flow parallel lineations that make up our Fs34, 36, 37, 39, 50, 52 and 53 as flow systems older than Late Wisconsinan (belonging to the Pelly swarm; pre-LGM). We classify the majority of these flowsets as stage 3 because they are comprised of well-preserved lineations with high parallel conformity that are deflected around the topography. A continuum of flow is also noted in some cases, for example, lineations within Fs39 merge with those in Fs60 towards the valley floor.

### 3.2. Ice retreat record

Meltwater channels frequently occur at high elevations (up to 1800 m asl) across the Cassiar and Omineca mountains (Gabrielse, 1988; Margold et al., 2013b; Dulfer and Margold, 2021). These channels often occur as narrow incisions in mountain ridges (Fig. 4 and Supplementary Fig. S1). Fig. 7a shows ice marginal positions of the CIS through the Cassiar, Omineca and Skeena mountains primarily reconstructed from glacial meltwater landforms. Successive ice marginal positions can be linked, indicating overall ice retreat towards the Coast and Skeena mountains in the west. However, it is challenging to connect ice marginal positions between valleys without chronological information.

### 3.3. Late Glacial readvances

A readvance of independent mountain glaciers during the Late Glacial is well documented in the geomorphic record of northern British Columbia with hundreds of well-preserved sharp-crested valley moraines located across the Cassiar and Omineca mountains (Ryder and Maynard, 1991; Lakeman et al., 2008a; Menounos et al., 2017). The glacial landform map of Dulfer and Margold (2021) documents the extensive regional distribution of these Late Glacial moraine ridges (purple stars in Fig. 7b). At 10 locations within the Cassiar and Omineca mountains, we find Late Glacial moraines are incised by lateral meltwater channels (green stars in Fig. 7b). At most locations, the moraines are sharp-crested and well-defined, with lateral meltwater channels incised into the moraine crests (Fig. 8a and b and Supplementary Fig. S2). This geomorphic relationship has been previously recognised by Lakeman et al. (2008a) in the Finlay River region of the Omineca Mountains.

## 4. Interpretation

### 4.1. Ice flow evolution

We interpret that the majority of the stage 1 flowsets were formed by north to northeasterly pre-LGM ice flow based on their morphology and cross-cutting relationships (Fig. 9a), although it is possible that they were formed during older glaciations. The exception is Fs20, which is oriented east-west and does not contain directional indicators. Thus, the time of formation of Fs20 is unknown.

Flowsets that have an orientation that is independent of the mountainous topography provide the best understanding of ice flow and ice sheet geometry at the maximum extent (Hughes et al., 2014). Therefore, we believe the stage 2 flowsets provide a glimpse of the local LGM ice flow pattern based on their high elevation and orientation that disregards topography (Fig. 9b). However, as we do not know the absolute timing of this ice flow it is possible that stage 2 flow occurred during the early stages of deglaciation rather than at the local LGM.

We interpret all stage 3 flowsets to be formed during the

deglaciation because they contain well preserved lineations that were produced by topographically controlled flow. Although, it can be difficult to determine the relative timing of these flowsets, ice flow reversals and cross-cutting relationships allow us to unravel the timing of ice flow on the western side of the study area. Consequently, we show the position of the ice divide shifted multiple times through the deglaciation (Fig. 9c–e).

We interpret that Fs36, 39, 52, and 53 were active early in the deglaciation (Fig. 9c), when the ice divide was still centered over the Cassiar Mountains. These flowsets display many of the characteristics of fast flowing ice, including highly convergent, topographically-controlled flow patterns, attenuated bedforms, and abrupt lateral margins that are typical of ice streams (Stokes and Clark, 1999; Margold et al., 2015). This configuration of these stage 3 flowsets resulted in an initial eastward migration of the ice divide from its LGM position and the formation of an ice divide near the Yukon-British Columbia border. With this configuration of flowsets it is possible that the ice divide could be located even further to the east, but, as ice flow over the northern Rocky Mountains has yet to be documented, we do not place it further eastwards at this time.

The ice flow reversal between southward flowing Fs52 and 53 and northward flowing Fs48, 51, and 54 indicates the ice divide then shifted westwards towards the Coast Mountains (Fig. 9d). This is supported by the distribution and orientation of ice contact deglacial landforms that show the overall ice retreat pattern towards the west (Fig. 7a). The ice flow reversal between southward flowing Fs21 and northward flowing Fs65 shows continued westward migration of the ice divide over the Coast Mountains, while the orientation of Fs1, 3, 4, 5, 10, 18 indicate that ice also retreated towards the Skeena Mountains during the late stages of deglaciation (Fig. 9e).

### 4.2. Evolution of the central sector of the Cordilleran Ice Sheet

#### 4.2.1. Ice sheet build-up

It has long been suggested that ice expanded outward from accumulation centers in the Coast, Cassiar and Skeena mountains, eventually coalescing to form the CIS (Davis and Mathews, 1944; Clague, 1980; Fulton, 1991; Ryder and Maynard, 1991; Clague and Ward, 2011). Thick glaciolacustrine sediments exposed in sedimentary sections along the banks of the Stikine River provide evidence that advancing glaciers from the Coast Mountains blocked the flow of the Stikine River during ice expansion, forming Glacial Lake Stikine (Fig. 10a; Ryder and Maynard, 1991; Spooner and Osborn, 2000). There is also evidence of additional transient ice-dammed lakes forming in eastward-draining valleys during ice advance, such as in the Dease River valley, where thick glaciolacustrine sediments are overlaid by till and esker sediment (Gabrielse, 1963). Therefore, stage 1 flowsets provide further evidence of ice expansion from the Coast Mountains (Fig. 10a). We did not find evidence of ice advance from the other mountain ranges in northern British Columbia as predicted by the conceptual model (Fulton, 1991; Clague et al., 2004; Clague and Ward, 2011) and numerical ice sheet modelling (Seguinot et al., 2016).

#### 4.2.2. LGM configuration

In northern British Columbia, we draw the local LGM ice divide centered over the Teslin Trench, west of the Cassiar Mountains, based on the distribution of stage 2 flowsets (Fig. 10b). The location of this ice divide aligns well with the northern branch of the LGM ice divide in the Yukon Territory, which follows the Cassiar Mountains into the Pelly and Selwyn mountains (see Fig. 1 for location; Jackson et al., 1991; Bond and Kennedy, 2005; Bond, 2007; Turner et al., 2008). However, our flowsets do not conform to a

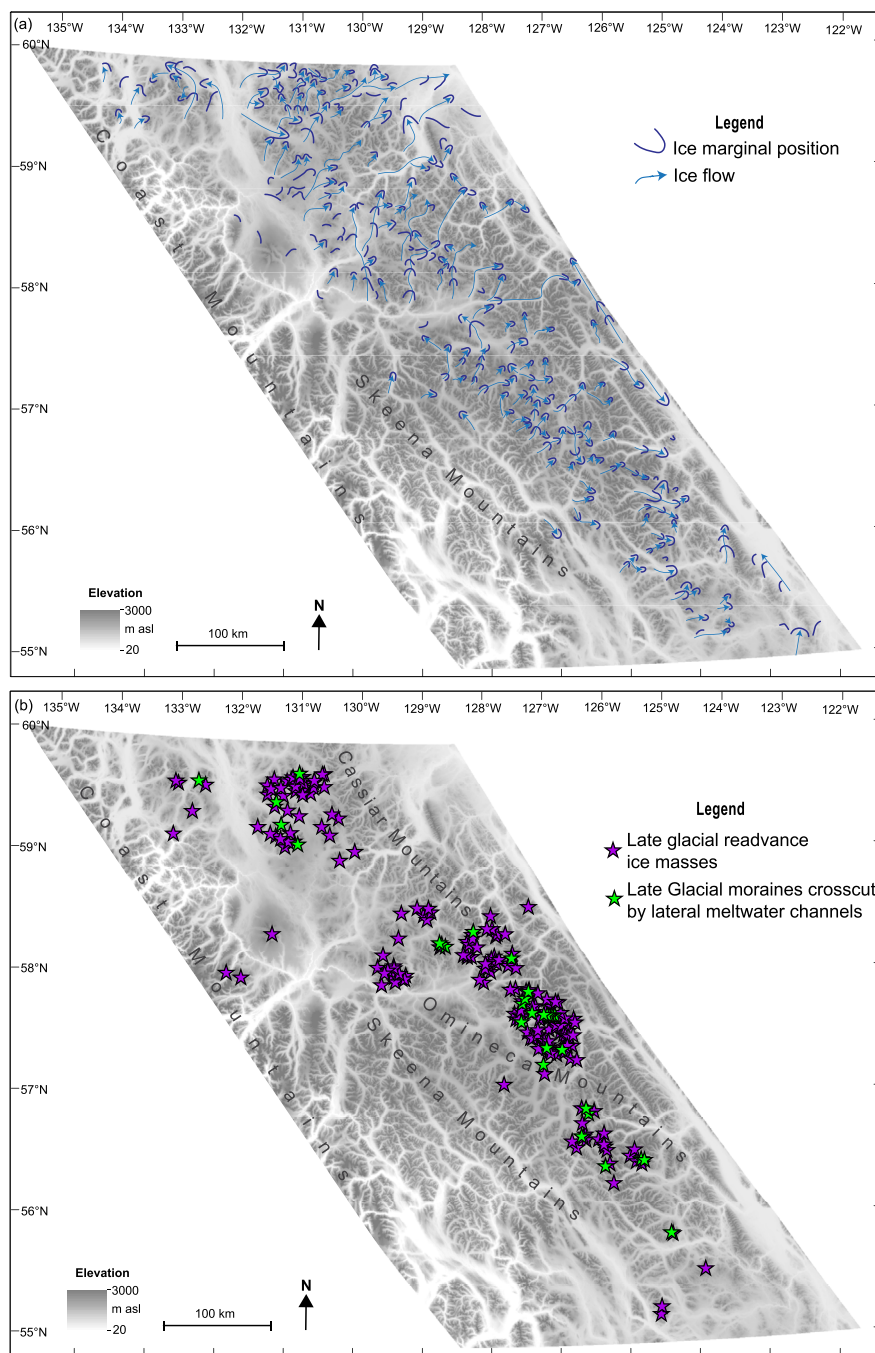


**Fig. 7.** (a) Retreat pattern of the CIS through the Cassiar, Omineca and Skeena mountains in northern British Columbia. Ice margins are shown by dark blue lines and light blue arrows show the ice flow direction for a series of retreating ice margins. (b) Distribution of mountain-centered Late Glacial readvance glaciers, ice caps, and ice fields (purple stars) interpreted from the Late Glacial readvance moraines mapped by Dulfer and Margold (2021). Green stars show locations where Late Glacial moraines are incised by lateral and submarginal meltwater channels.

western branch of the LGM ice divide extending towards the St. Elias Mountains in northern British Columbia (Clague and Ward, 2011). Such a western ice divide branch may have been located further north at the LGM. In central British Columbia, Stumpf et al. (2000) infer a reversal in ice flow east of the Coast Mountains at the LGM and a similar change in ice flow can be seen between northward flowing stage 1 Fs35, 38, and 57 and westward flowing stage 2 Fs50. Additionally, stage 2 Fs19, 16, and 63 show ice flow towards the northern Rocky Mountains at the LGM. Ice flow across this part

of the Rocky Mountains has not been recorded, and thus, requires further investigation.

#### 4.2.3. Deglacial configuration

Cosmogenic nuclide ages indicate ice began to retreat along the Pacific coast at ~18 ka and was still at the mainland coastline by ~14 ka (Darvill et al., 2018; Darvill et al. in press; Lesnek et al., 2018, 2020). Ice retreat across the Rocky Mountains occurred after ~16 ka (Dulfer et al., 2021, Fig. 3). Subsequent ice sheet configuration



**Fig. 8.** Example of the interaction between CIS outlet glaciers and independent mountain glaciers interpreted from the glacial landform record. (a) Tandem X-derived hillshade imagery (German Aerospace Center, 2018) and (b) Planet Team (2017) satellite imagery showing two Late Glacial moraines cross-cut by lateral and submarginal meltwater channels. Other examples of this cross-cutting relationship are given in Supplementary Fig. S2. (c) Tandem X-derived hillshade imagery showing the broader area (white box shows location of a and b) and (d) glacial geomorphological mapping from Dulfer and Margold (2021). All of the Late Glacial moraines are crosscut by lateral and submarginal meltwater channels. (e) and (f) Schematic diagrams showing how CIS outlet glaciers and independent mountain glaciers responded to Late Glacial cooling. (e) Stage 1: as the CIS is retreating independent glaciers advance into high-altitude ice free areas during cooling. (f) Stage 2: CIS outlet glaciers responded to this cooling and later advanced over the Late Glacial moraines creating the cross-cutting lateral meltwater channels. The extent of the independent mountain glaciers at this time is unknown.

during the Bølling-Allerød interstadial (14.6–12.9 ka) is enigmatic. Recent studies of the CIS based on GIA analysis conclude that the ice sheet underwent substantial melting during the Bølling-Allerød warming, potentially losing up to half of its mass (Peltier et al., 2015; Lambeck et al., 2017; Menounos et al., 2017). However, while geochronological data are sparse within the interior of the ice sheet, they indicate that the CIS still covered a substantial area during the early part of the Bølling-Allerød interstadial (Fig. 10c;

Menounos et al., 2017; Darvill et al., 2018; Dulfer et al., 2021).

The glacial landform record of the central sector of the CIS provides some insight into the nature of deglaciation. The high elevation meltwater channels show that the peaks became ice free ahead of the valleys (Supplementary Fig. S1), while the remaining ice contact landforms show the active retreat of outlet glaciers (Fig. 7a). It follows that the response of the interior of the CIS may have been similar to the response of the southern dome of the

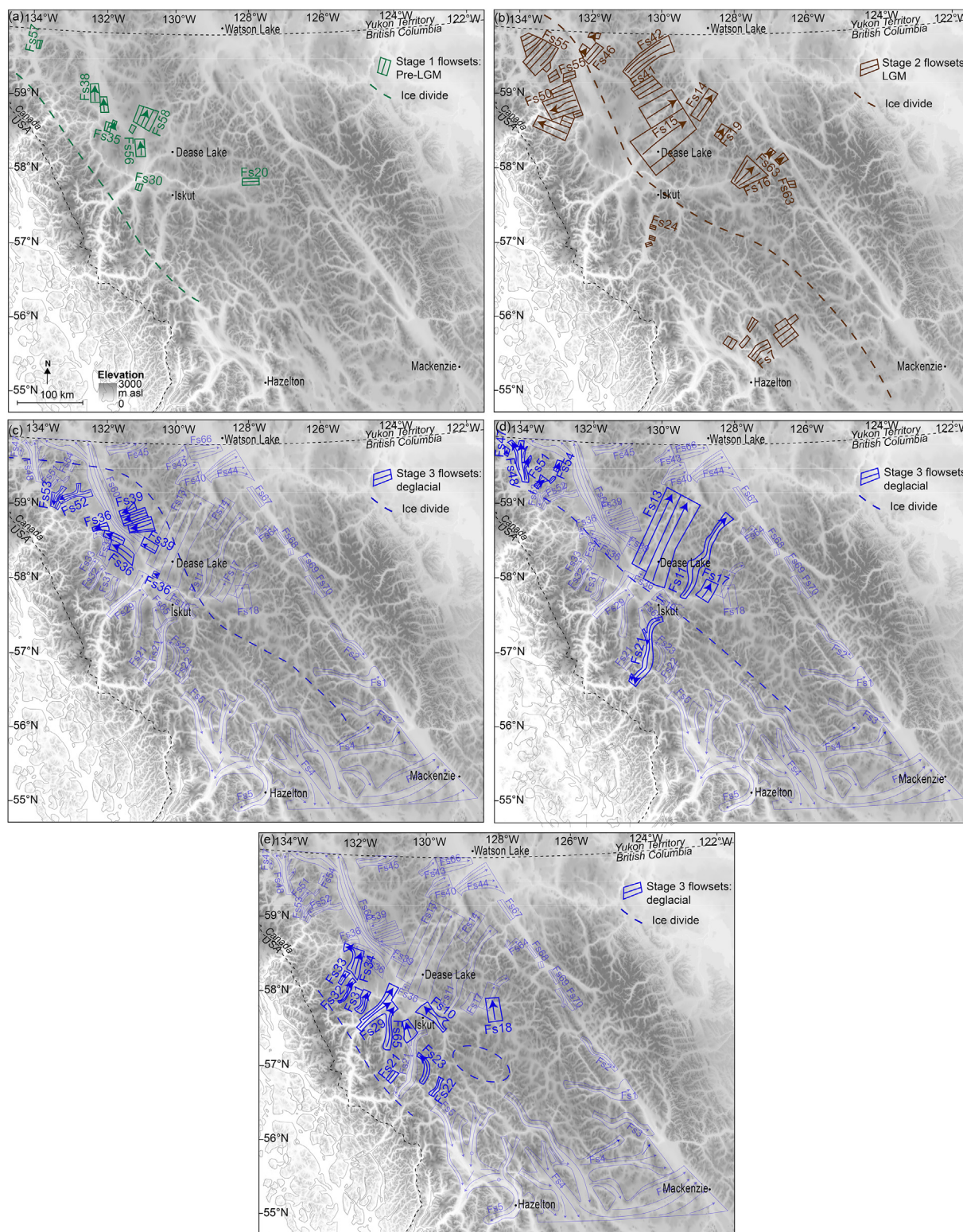


**Fig. 9.** Reconstruction of consecutive ice divide positions based on the flowset record. (a) The orientation of stage 1 Fs38, 35, 36 and 58 indicate an ice divide was located over the northern Coast Mountain prior to the LGM. (b) Reconstruction of the ice divide at, or close to, the LGM based on the distribution and orientation of Stage 2 flowsets. (c to e) Reconstruction of the ice divide during successive stage of deglaciation based on the distribution, orientation and morphology of flowsets. The flowsets that underpin the interpretation are shown in bold. It is likely that other Stage 3 flowsets were active in the south and east during each of these stages but their relative position and timing is unknown.

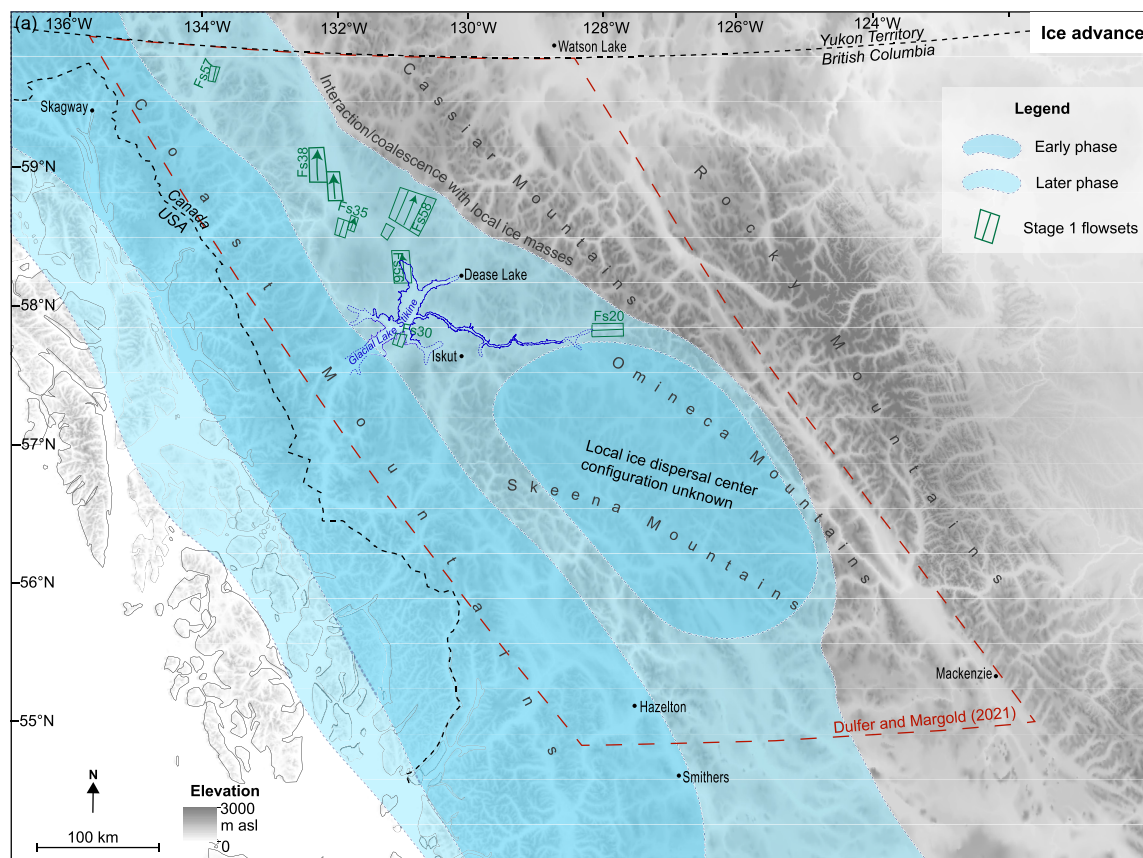


**Fig. 10.** (a) Reconstruction of the CIS during the ice advance phase. Initially, ice advance from the Coast Mountains blocked the drainage of the Stikine River forming Glacial Lake Stikine (early phase). The extent of Glacial Lake Stikine has been drawn from [Ryder and Maynard \(1991\)](#) based on the distribution of thick glaciolacustrine sediments. During this stage an ice dispersal center was also likely located over the Skeena Mountains ([Stumpf et al., 2000](#)) but the ice configuration there is unknown and there is no support in our data for this configuration. Stage 1 flowsets record a continued advance of the CIS from the Coast and Skeena Mountains (later phase). The red dashed box shows the extent of the glacial landform map of [Dulfer and Margold \(2021\)](#). (b) Configuration of the ice sheet at the LGM based on the distribution of stage 2 flowsets. Position of the ice divide is given by the blue line (solid line where it is based on an abundance of flowsets, dashed elsewhere) and ice flow directions by blue dashed arrows. (c) Hypothetical ice extent when CIS pulls back from the Rocky Mountains. Approximate positions of the ice divide and generalized flowlines are shown with dark blue. Selected stage 3 flowsets that may have been active at this time are shown with light blue dashed lines. Cosmogenic nuclide ages from [Menounos et al. \(2017\)](#), [Lesnek et al. \(2018, 2020\)](#), and [Dulfer et al. \(2021\)](#) are shown by black stars. All ages have been corrected for GIA and the ages in bold have also been corrected for snow shielding. (d) Extent of the CIS during a Late Glacial readvance (light blue) and the generalized distribution of mountain centered readvance glaciers (dark blue). The selected cosmogenic nuclide ages are from [Lesnek et al. \(2018, 2020\)](#), [Menounos et al. \(2017\)](#) and [Margold et al. \(2014\)](#). All ages have been corrected for GIA and the ages in bold have also been corrected for snow shielding. The radiocarbon dates are from [Fulton \(1971\)](#), [Clague \(1984\)](#) and [Lakeman et al. \(2008b\)](#). Ages that are marked with asterisks are inferred to relate to a Late Glacial readvance of alpine glaciers. (e) Hypothetical ice extent in the last stage of deglaciation. The orientations of deglaciation flowsets indicate that the CIS was split into at least two separate ice bodies: one centered over the Skeena Mountains and the other over the northern Coast Mountains. The relative and absolute timings of the demise of these ice bodies is unknown. (For interpretation of the references to colour in this figure legend, the reader is referred to the Web version of this article.)

Fennoscandian Ice Sheet (FIS) in the Late Glacial period, with a recent study by [Lane et al. \(2020\)](#) finding that both thinning and ice marginal retreat were substantial both during the Bølling-Allerød warming and after the YD. However, the rate of thinning of the CIS during this period of rapid climate change still needs to be quantified.

#### 4.2.4. Late Glacial ice configuration

A Late Glacial readvance of independent mountain glaciers into high altitude ice free areas is well documented in northern British Columbia ([Lakeman et al., 2008a, 2008b](#); [Menounos et al., 2017](#); [Dulfer and Margold, 2021](#)). We interpret the cross-cutting relationship of Late Glacial readvance moraines that are incised with lateral and submarginal meltwater channels ([Figs. 7b and 8d](#)) as a differential response of ice masses to regional cooling. The independent mountain glaciers advanced first and in some places merged with outlet glaciers of the CIS ([Lakeman et al., 2008a](#)).

Outlet glaciers of the CIS also responded to this cooling by readvancing, but with a lag time due to its larger size. Hence, at some locations advancing CIS outlet glaciers locally overran the Late Glacial moraines of independent glaciers ([Fig. 8f](#)). The preservation of these moraines requires the CIS outlet glaciers to have been polythermal or cold-based with ice advancing by internal deformation rather than basal sliding ([Kleman, 1994](#); [Davis et al., 2006](#); [Fabel et al., 2006](#)). The lateral and submarginal meltwater channels were then eroded into the Late Glacial moraines during the final retreat of the outlet glaciers.

The distribution of mountain-centered readvance glaciers, ice caps, and ice fields forms a distinctive band through the Cassiar and Omineca mountains ([Fig. 7b](#)) and provides important information about the ice configuration during the Late Glacial. Firstly, these independent mountain glaciers can only form on peaks that are free of the CIS ([Lakeman et al., 2008a](#); [Menounos et al., 2017](#)), and thus, their presence delineates areas that were already deglaciated at the



Fig. 10. (continued).

time of formation. Conversely, as there is a strong west-east precipitation gradient across British Columbia with the highest rainfall falling over the mountains to the west (Ryder, 1989), the lack of independent mountain glaciers to the west of the mapped distribution indicates that these areas must have been covered by the CIS at this time, prohibiting independent mountain glaciers from forming. Thus the distribution of independent mountain-centered glaciers defines a maximum eastern extent of the CIS during the Late Glacial (Fig. 10d). Furthermore, we suggest that the location of the mountain-centered glacier readvance moraines that are incised by lateral meltwater channels defines the location of some of the outlet glaciers of the CIS at this time.

Lake sediments deposited when readvance moraines produced by alpine glaciers began to block natural drainage pathways have been radiocarbon dated, giving a minimum age for the readvance of ~10 ka (Lakeman et al., 2008b, Fig. 10d). Additionally, three readvance moraines produced by alpine glaciers have been <sup>10</sup>Be exposure dated, giving weighted mean exposure ages of 11.3 ± 0.3 ka at Tuya Lake (GIA and snow cover corrected), 11.9 ± 0.4 ka at Grey Lake (GL; GIA corrected; snow cover correction not applicable) and 10.3 ± 0.3 ka at Crushing Lake (GIA corrected; snow cover correction not possible; Fig. 10d; Menounos et al., 2017). Although uncertainties make it difficult to determine whether individual landforms correlate with millennial-scale climate events (Balco, 2020), these exposure ages could be consistent with the Late Glacial readvances occurring within the YD stadial (Menounos et al., 2017).

#### 4.2.5. Final ice configuration

The ice configuration during the final stages of the deglaciation is given by a number of stage 3 flowsets (e.g. Fs21, 23, 29, 31, and 34) that indicate an ice body was centered on the northern Coast Mountains while other stage 3 flowsets (e.g. Fs10, 18 and 65) require an ice body centered over the Skeena Mountains (Fig. 10e). This reconstruction fits well with the numerical ice sheet model of Seguinot et al. (2016; see snapshot for 10 ka in Fig. 2i), however, the relative timing of the demise of each of these ice bodies is unknown. It should be noted that there is no evidence that a glacial lake was formed in the Stikine River valley during deglaciation, suggesting deglaciation of this river valley was rapid.

### 5. Discussion

#### 5.1. Deglaciation style

As noted in Dulfer and Margold (2021), there is a large difference in the glacial landform assemblages in the Cassiar and Omineca mountains to the east, where thousands of lateral and submarginal meltwater channels have been mapped, and the Skeena and Coast Mountains to the west where meltwater landforms are absent and this reflects differences in the style of ice retreat.

To the east, channels eroded into mountain ridges by meltwater across the Cassiar and Omineca mountains indicate high elevation areas became deglaciated ahead of valleys, causing emergence of numerous nunataks around the periphery of the ice sheet during deglaciation. Recognition of vertical downwasting has led previous studies to conclude that CIS deglaciation was dominated by

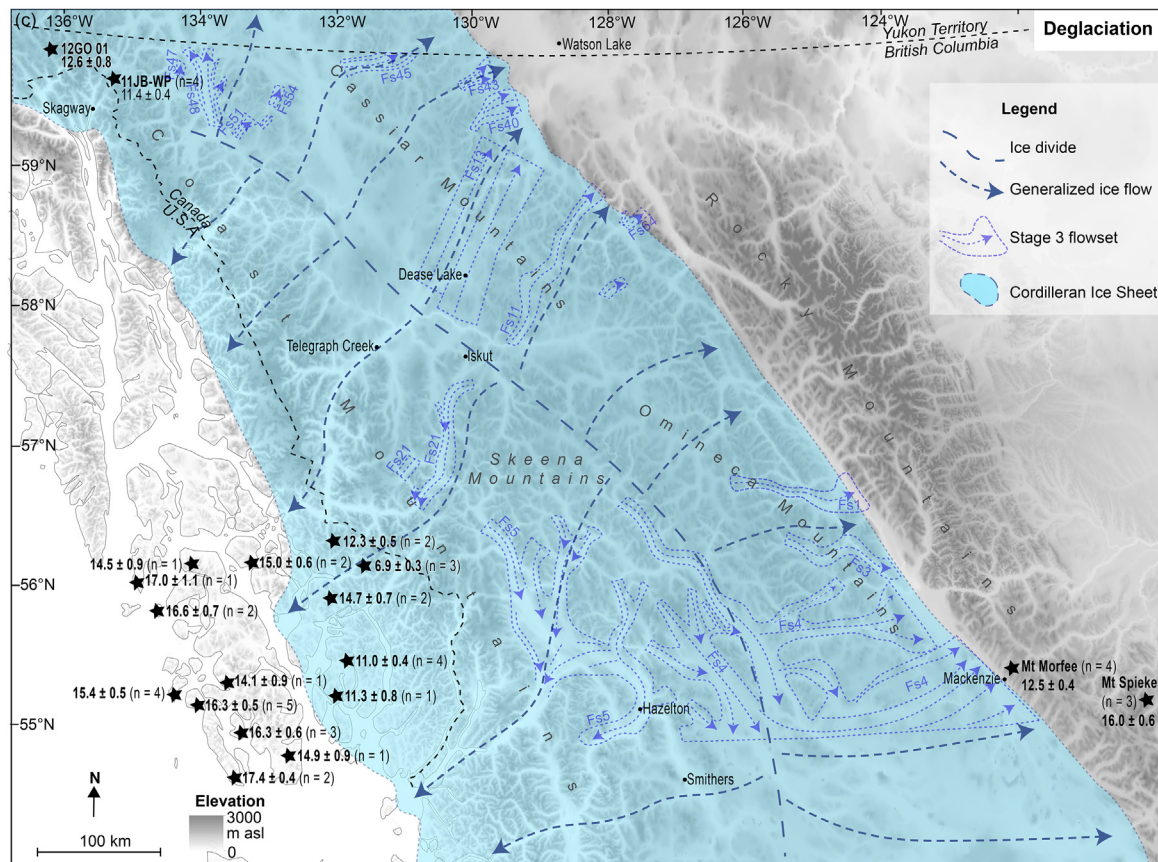


Fig. 10. (continued).

regional ice stagnation but without clarity over spatial and temporal variability (Davis and Mathews, 1944; Fulton, 1991). However, suites of ice contact landforms, such as abundant lateral and submarginal meltwater channels, kame terraces, and perched deltas indicate CIS outlet glaciers actively retreated through the mountains of northern British Columbia, similar to the southern sectors of the CIS (Margold et al., 2013b; Perkins and Brennand, 2015; Sacco et al., 2017).

Furthermore, the abundance of lateral and submarginal meltwater channels and overall lack of CIS outlet glacier moraines within the Cassiar and Omineca mountains suggests a cold-based or polythermal regime, because although lateral meltwater channels are not exclusively formed under cold-based thermal conditions (Syverson and Mickelson, 2009), a frozen bed can prohibit meltwater from draining englacially and subglacially (Dyke, 1993; Kleman and Borgström, 1996; Greenwood et al., 2007, 2016).

To the south and west of the Skeena Mountains, the landform assemblage consists of extensive streamlined terrain (e.g. Fs4, 5, and 21) that is characteristic of fast flowing, warm-based ice (Borgström, 1999; Glasser and Bennett, 2004). However, with the exception of the Kitimat Trough, where large volumes of sand and gravel were deposited as ice-contact and proglacial deltas (Clague, 1980, 1985), there is an overall lack of deglacial meltwater landforms that are also indicative of warm-based ice. We suggest that the Holocene and present-day climate influenced the preservation of these depositional landforms, with the high precipitation rates along the Coast Mountains causing the deglacial and proglacial sediments to be reworked.

These spatial variations in the landform assemblage across

northern British Columbia share many similarities to the landform record surrounding the Scandinavian Mountains, whereby suites of lateral and submarginal meltwater channels are found to the east, e.g. within the Transtrand Mountains in western Sweden (Kleman et al., 1992), while the landscape is heavily scoured and streamlined to the west of the Scandinavian Mountains in southwestern Norway (Mangerud et al., 2019). This suggests that the deglacial dynamics of the CIS may have been more similar to that of the FIS than previously thought.

## 5.2. Comparison with other readvances across western North America

### 5.2.1. Readvances of the Cordilleran Ice Sheet

Readvances of the CIS during the deglaciation have been recorded in a number of locations both in the interior and along the Pacific Coast. In the Yukon Territory, a readvance of outlet glaciers of the Cassiar Lobe of the CIS into the Pelly Mountains has been documented by Kennedy and Bond (2004; see Fig. 1 for location). While this readvance has not been dated, it is likely that it occurred early in the deglaciation when the CIS was extensive enough to cover the northern Cassiar Mountains.

Multiple moraines have been mapped in the Kitimat fiord system (Shaw et al., 2017), and ice marginal accumulations of sand, gravel, and till continue into the Kitimat trough, marking periods of glacier stabilization or advance during the deglaciation (Clague, 1984, 1985). Again, these ice marginal positions have yet to be dated, however, radiocarbon ages from shells within nearby glaciomarine sediments constrain the timing of deglaciation of the

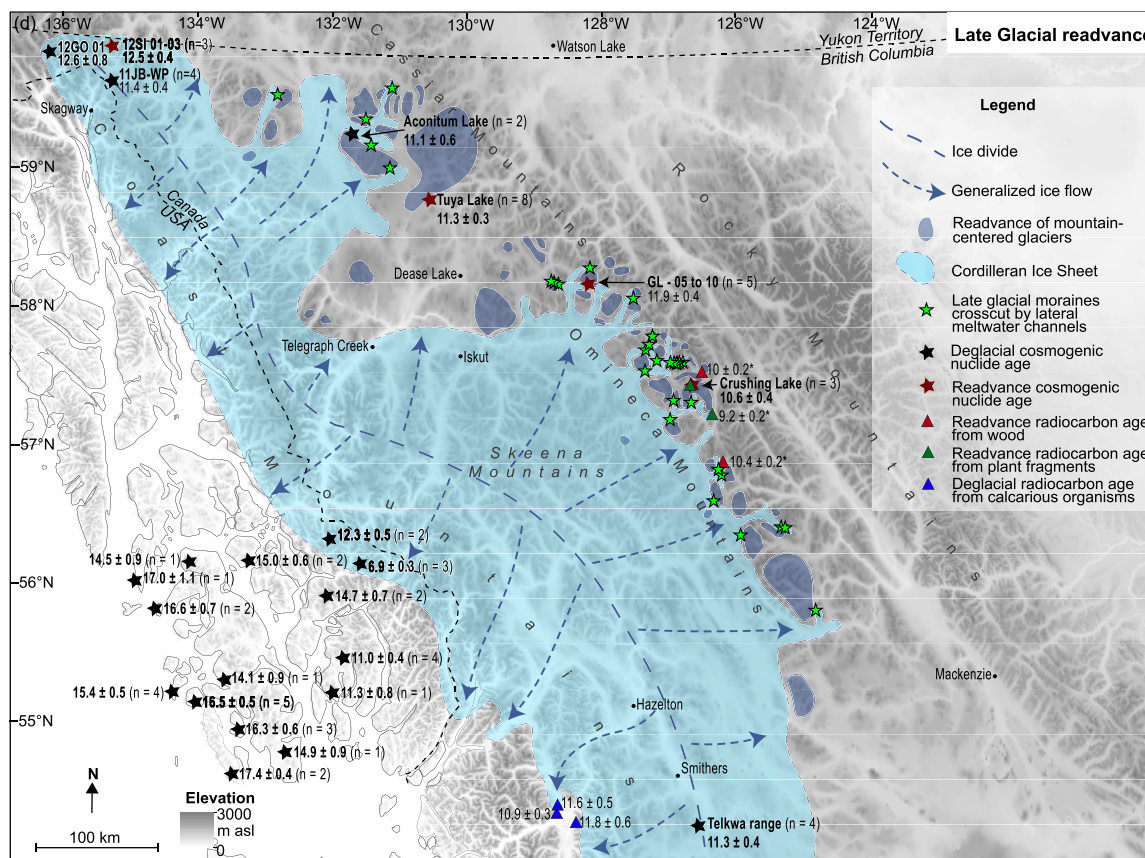


Fig. 10. (continued).

Kitimat trough to  $11.8 \pm 0.6$  cal ka BP (GSC-523; Clague, 1984, Fig. 10d).

A readvance of outlet glaciers in the Squamish River Valley in southern British Columbia occurred between  $12.6 \pm 0.1$  and  $12.1 \pm 0.5$  cal ka BP (GSC-6610 and GSC-6236 respectively; Friele and Clague, 2002), and at least three readvances, known as the Sumas readvances, occurred in the Fraser River Valley, a short distance south of Squamish. These readvances are summarized in Clark and Clague (2021) as: (1) an early maximum readvance at 14.6 cal ka BP; (2) a second and more regionally extensive readvance between 14.2 and 13.0 cal ka BP; and (3) a lesser final readvance between 13.0 and 11.2 cal ka BP (Clague et al., 1997; Kovanen, 2002; Kovanen and Easterbrook, 2002; Clark and Clague, 2021). The first two Sumas readvances fall within the Bølling-Allerød warming and could have occurred during one of the multiple short-lived cooling events seen in the Greenland ice core records (GI-1 b or d; Rasmussen et al., 2014) or they may be related to changes in the ice sheet dynamics caused by other factors such as glacier geometry, bed topography, ocean temperatures, and sea level fluctuations (Clague et al., 1997; Clark and Clague, 2021). The last Sumas readvance and the readvance of outlet glaciers within the Squamish River Valley both occur within the YD stadial and these readvances may have occurred at the same time as the readvance of outlet glaciers we record along the eastern margin of the CIS.

### 5.2.2. Readvances of independent mountain glaciers

The readvance of independent mountain glaciers during the Late Glacial and Early Holocene is well documented in other areas

of western North America (Menounos et al., 2009). In the central Rocky Mountains there was a regionally extensive advance of cirque glaciers, locally termed the Crowfoot advance (Luckman and Osborn, 1979; Reasoner et al., 1994; Osborn and Gerloff, 1997). This advance has been dated using plant material from lake sediments, giving an age range between  $13.2 \pm 0.4$  cal ka BP and  $11.5 \pm 0.3$  cal ka BP (CAMS3065 and CAMS3063 respectively; Reasoner et al., 1994).

Along the Pacific Coast a readvance of cirque glaciers occurred in the northern Cascade Mountains at  $12.9 \pm 0.4$  ka (BL-BG-03 to 07; GIA and snow cover corrected; Marcott et al., 2019), in the southern Coast Mountains between  $10.2 \pm 0.5$  ka (sample ID BI-1 and BO-1; only GIA corrected) and  $11.3 \pm 0.3$  ka (sample ID FE10-1 to 4; only GIA corrected) and in the St. Elias Mountains at  $11.2 \pm 0.5$  ka (GIA and snow cover corrected; Menounos et al., 2017). Readvances of alpine glaciers are also noted in the Ahklun Mountains of Alaska at  $12.2 \pm 0.3$  ka (outer Mt Wasley moraine) and  $11.7 \pm 0.3$  ka (inner Mt Wasley moraine; only GIA corrected; Briner et al., 2002; Young et al., 2019). Although there is some variability in the timing of these readvances, most of them fall within the YD stadial, which aligns with the ages obtained from Late Glacial readvance moraines within our study area.

### 5.3. Regional climate during the Late Glacial

Alkenone-based sea-surface-temperature (SST) estimates and a planktonic-foraminiferal Mg/Ca-based ocean temperature record from a core west of Vancouver Island show that the SST oscillated multiple times through the Late Glacial period. These oscillations

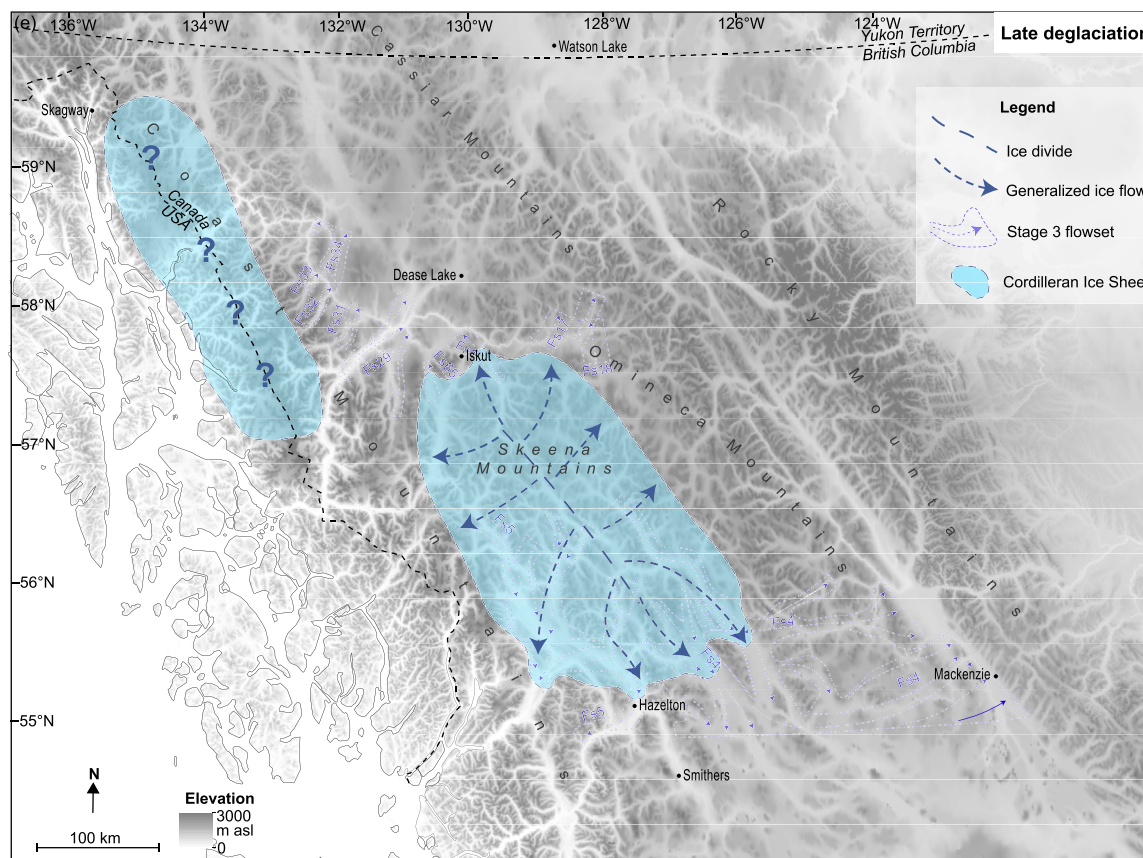


Fig. 10. (continued).

correspond well to the  $\delta^{18}\text{O}$  record within the Greenland ice cores (Kienast and McKay, 2001; Taylor et al., 2014), indicative of dynamic coupling of the North Pacific and North Atlantic climates during this period of rapid climate changes (Praetorius and Mix, 2014; Walczak et al., 2020).

Alkenone SST estimates indicate the largest climate deteriorations along the Pacific Coast of North America occurred during the YD stadial, when temperatures dropped by 3 °C–4 °C (Kienast and McKay, 2001; Praetorius et al., 2015) and palynological evidence from the same region supports a regional cooling event during the YD stadial (Engstrom et al., 1990; Mathewes, 1993; Mathewes et al., 1993; Hetherington and Reid, 2003; Lacourse, 2005). Therefore, based on the geomorphological evidence of an extensive regional readvance of both mountain-centered glaciers and outlet glaciers of the CIS in northern British Columbia (Dulfer and Margold, 2021) and the available quantitative chronology (Lakeman et al., 2008b; Menounos et al., 2017), we suggest that the reconstructed ice sheet extent shown in Fig. 10d represents the ice extent of the CIS at the end of the YD stadial.

## 6. Future work

Here we highlight a number of outstanding challenges in regards to understanding the glacial history of the CIS through the last glacial cycle. These challenges include:

- Gaining a better understanding of the ice sheet build-up stage as well as the ice extent during MIS 3, 4 and 6.
- Quantifying the rate of ice sheet thinning during deglaciation.

- Reconstructing the evolution of ice-dammed lakes during deglaciation.
- Further quantitative dating of both the deglaciation of the central sector/last remnant of the CIS and of the Late Glacial readvance moraines.

These challenges can be addressed by gathering further empirical data and improving the performance of numerical simulations. In particular, the focus should be on increasing the resolution of numerical models, improving the climate forcing data and reconciling the models with available empirical and proxy data to better capture the complex ice dynamics during the Late Glacial.

## 7. Conclusions

The glacial landform record of northern British Columbia allows us to unravel advance and retreat dynamics of the central sector of the CIS, beneath the local LGM ice divide. Seventy glacial flowsets have been mapped and the majority of these flowsets have been categorized based on morphology, elevation, orientation and cross-cutting relationships into three stages. Stage 1 and 2 flowsets likely formed by pre-LGM and LGM ice flow respectively, and the location of the LGM ice divide aligns well with the current understanding of the CIS at its LGM. Stage 3 flowsets were formed by deglacial ice-flow and their distribution and orientation indicates the ice divide migrated multiple times throughout the deglaciation. Combined with the distribution of CIS outlet glacier moraines and glacial meltwater landforms, we map an overall ice retreat pattern that proceeded westwards towards the Coast and Skeena

mountains.

We map the regional distribution of independent mountain glaciers, ice caps, and ice fields, that regrew in high elevation areas in the Late Glacial and identify that some of these moraines are incised by lateral and submarginal meltwater channels formed along the CIS margins. We use this glacial landform relationship to show that CIS outlet glaciers also advanced in the Late Glacial and this allows us to map the maximum extent of the eastern margin of the CIS during late stages of deglaciation for the first time. We suggest, based on the available quantitative chronology and climate proxy data, that this readvance likely occurred during the YD stadial, however, further chronological controls are required to confirm the timing.

## Funding

This research was supported by the Charles University Grant Agency under grant number GAUK 432119 awarded to HED and the Czech Science Foundation under grant number 19-21216Y awarded to MM.

## Data availability

We provide shapefiles of the seventy flowsets mapped during this study, which can be downloaded at <http://doi.org/10.6084/m9.figshare.19234803>. We also provide a shapefile of generalized ice flow indicators that represents an intermediate step of classification between the streamlined features and the flowsets themselves.

## Declaration of competing interest

The authors declare that they have no known competing financial interests or personal relationships that could have appeared to influence the work reported in this paper.

## Acknowledgements

The authors thank Planet Lab who provided the high-resolution satellite imagery (4-band PlanetScope scenes) through their education and research program and the German Aerospace Center for awarding us a TandDEM-X Science DEM project, which allowed us to download high resolution Tan-DEM X DEM (0.4 arc second resolution) covering 100,000 km<sup>2</sup>. April Dalton is thanked for reviewing the manuscript and providing the calibrated radiocarbon ages. Jakob Heyman is thanked for providing the GIA-corrected cosmogenic nuclide exposure ages. We thank Gregory Ruetenik for extracting the snow depth and density data and Alia Lesnek, Shaun Marcott and Shan Ye are thanked for providing their boulder height data. Stephen Livingstone and one anonymous reviewer are thanked for providing insightful and constructive suggestions that helped to improve the manuscript.

## Appendix A. Supplementary data

Supplementary data to this article can be found online at <https://doi.org/10.1016/j.quascirev.2022.107465>.

## References

Arnold, H., Ferbey, T., Hickin, A.S., 2016. Ice-flow Indicator Completion, British Columbia and Yukon. Geological Survey of Canada. <https://doi.org/10.4095/298865>. Open File 8083.

Balco, G., 2020. Glacier change and paleoclimate applications of cosmogenic nuclide exposure dating. *Annu. Rev. Earth Planet Sci.* 48 (1), 21–48. <https://doi.org/10.1146/annurev-earth-081619-052609>.

Balco, G., Stone O, J., Lifton A, N., Dunai J, T., 2008. A complete and easily accessible

means of calculation surface exposure ages or erosion rates from <sup>10</sup>Be and <sup>26</sup>Al measurements. *Quat. Geochronol.* 3, 174–195. <https://doi.org/10.1016/j.quageo.2007.12.001>.

Bond, J., 2007. Late Wisconsinan McConnell glaciation of the Bug Salmon range, Yukon. In: Emond, D.S., Lewis, L.L., Wenston, L.H. (Eds.), *Yukon Exploration and Geology 2006*. Yukon Geological Survey, pp. 105–122.

Bond, J., Kennedy, K.E., 2005. Late Wisconsinan McConnell ice-flow and sediment distribution patterns in the Pelly mountains, Yukon. In: Emond, D.S., Lewis, L.L., Bradshaw, G.D. (Eds.), *Yukon Exploration and Geology 2004*. Yukon Geological Survey, pp. 67–82.

Borchers, B., Marrero, S., Balco, G., Caffee, M., Goehring, B., Lifton, N., Nishiizumi, K., Phillips, F., Schaefer, J., Stone, J., 2016. Geological calibration of spallation production rates in the CRONUS-Earth project. *Quat. Geochronol.* 31, 188–198. <https://doi.org/10.1016/j.quageo.2015.01.009>.

Borgström, I., 1999. Basal ice temperatures during late Weichselian deglaciation: comparison of landform assemblages in west-central Sweden. *Ann. Glaciol.* 28, 9–15. <https://doi.org/10.3189/172756499781821904>.

Borsellino, R., Shulmeister, J., Winkler, S., 2017. Glacial geomorphology of the Brabazon and Butler downs, Rangitata valley, south Island, New Zealand. *J. Maps* 13 (2), 502–510. <https://doi.org/10.1080/17445647.2017.1336122>.

Brennard, T., Perkins, A.J., 2017. The deglacial landscape of the southern Fraser Plateau. In: Slaymaker, O. (Ed.), *Landscape and Landforms of Western Canada*. Springer International Publishing, pp. 277–290.

Brennard, T.A., 2000. Deglacial meltwater drainage and glaciodynamics: inferences from Laurentide eskers, Canada. *Geomorphology* 32, 263–293. [https://doi.org/10.1016/S0169-555X\(99\)00100-2](https://doi.org/10.1016/S0169-555X(99)00100-2).

Briner, J.P., Kaufman, D.S., Werner, A., Caffee, M., Levy, L., Manley, W.F., Kaplan, M.R., Finkel, R.C., 2002. Glacier readvance during the late glacial (younger Dryas?) in the Ahklun mountains, southwestern Alaska. *Geology* 30 (8). [https://doi.org/10.1130/0091-7613\(2002\)030<0679:Grdtlg>2.0.Co;2](https://doi.org/10.1130/0091-7613(2002)030<0679:Grdtlg>2.0.Co;2).

Brown, T.C., 1931. Kames and kame terraces of central Massachusetts. *GSA Bull.* 42 (2), 467–480. <https://doi.org/10.1130/GSAB-42-467>.

Chandler, B.M.P., Lovell, H., Boston, C.M., Lukas, S., Barr, I.D., Benediktsson, Í.Ö., Benn, D.I., Clark, C.D., Darvill, C.M., Evans, D.J.A., Ewertowski, M.W., Loibl, D., Margold, M., Otto, J.-C., Roberts, D.H., Stokes, C.R., Storrar, R.D., Stroeven, A.P., 2018. Glacial geomorphological mapping: a review of approaches and frameworks for best practice. *Earth Sci. Rev.* 185, 806–846. <https://doi.org/10.1016/j.earscirev.2018.07.015>.

Clague, J.J., 1980. Late Quaternary Geology and Geochronology of British Columbia. Part 2: Summary and Discussion of Radiocarbon-Dated Quaternary History. Canadian Government Publishing Centre, Ottawa, Canada. <https://doi.org/10.4095/119439>. Geological Survey of Canada paper 80-35.

Clague, J.J., 1984. Quaternary Geology and Geomorphology, Smithers-Terrace-Prince Rupert Area. Canadian Government Publishing Centre, Ottawa, Canada. <https://doi.org/10.4095/119547>. British Columbia. Geological Survey of Canada Memoir 413.

Clague, J.J., 1985. Deglaciation of the Prince Rupert-Kitimat area, British Columbia. *Can. J. Earth Sci.* 22, 256–265. <https://doi.org/10.1139/e85-022>.

Clague, J.J., Mathewes, R.W., Ager, T.A., 2004. Environments of north-western North America before the last glacial maximum. In: Madsen, D. (Ed.), *Entering America: Northeast Asia and Beringia before the Last Glacial Maximum*. University of Utah Press.

Clague, J.J., Mathewes, R.W., Guilbault, J.P., Hutchinson, I., Ricketts, B.D., 1997. Pre-Younger Dryas resurgence of the southwestern margin of the Cordilleran ice sheet, British Columbia, Canada. *Boreas* 26 (3), 261–278. <https://doi.org/10.1111/j.1502-3885.1997.tb00855.x>.

Clague, J.J., Ward, B., 2011. Pleistocene glaciation of British Columbia. In: Ehlers, J., Gibbard, P.L., Hughes, P.D. (Eds.), *Quaternary Glaciations - Extent and Chronology - A Closer Look*. Elsevier Developments in Quaternary Science, pp. 563–573. <https://doi.org/10.1016/b978-0-444-53447-7.00044-1>.

Clark, D.H., Clague, J.J., 2021. Glaciers, isostasy, and eustasy in the Fraser Lowland: a new interpretation of late Pleistocene glaciation across the International Boundary. In: Waitt, R.B., Thackray, G.D., Gillespie, A.R. (Eds.), *Untangling the Quaternary Period—A Legacy of Stephen C. Porter*, vol. 548. Geological Society of America. [https://doi.org/10.1130/2020.2548\(13\)](https://doi.org/10.1130/2020.2548(13)).

Dalton, A.S., Margold, M., Stokes, C.R., Tarasov, L., Dyke, A.S., Adams, R.S., Allard, S., Arends, H.E., Atkinson, N., Attig, J.W., Barnett, P.J., Barnett, R.L., Batterson, M., Bernatchez, P., Borns, H.W., Breckenridge, A., Briner, J.P., Brouard, E., Campbell, J.E., Carlson, A.E., Clague, J.J., Curry, B.B., Daigneault, R.-A., Dubé-Loubert, H., Easterbrook, D.J., Franzi, D.A., Friedrich, H.G., Funder, S., Gauthier, M.S., Gowan, A.S., Harris, K.L., Hétu, B., Hooyer, T.S., Jennings, C.E., Johnson, M.D., Kehew, A.E., Kelley, S.E., Kerr, D., King, E.L., Kjeldsen, K.K., Knaeble, A.R., Lajeunesse, P., Lakeman, T.R., Lamothe, M., Larson, P., Lavoie, M., Loope, H.M., Lowell, T.V., Lusardi, B.A., Manz, L., McMartin, I., Nixon, F.C., Occhietti, S., Parkhill, M.A., Piper, D.J.W., Pronk, A.G., Richard, P.J.H., Ridge, J.C., Ross, M., Roy, M., Seaman, A., Shaw, J., Stea, R.R., Teller, J.T., Thompson, W.B., Thorleifson, L.H., Utting, D.J., Veillette, J.J., Ward, B.C., Weddle, T.K., Wright, H.E., 2020. An updated radiocarbon-based ice margin chronology for the last deglaciation of the North American Ice Sheet Complex. *Quat. Sci. Rev.* 234, 106223. <https://doi.org/10.1016/j.quascirev.2020.106223>.

Darvill, C.M., Menounos, B., Goehring, B.M., Lesnek, A.J., in press. Cordilleran Ice Sheet stability during the last deglaciation. *Geophys. Res. Lett.*

Darvill, C.M., Menounos, B., Goehring, B.M., Lian, O.B., Caffee, M.W., 2018. Retreat of the western Cordilleran ice sheet margin during the last deglaciation. *Geophys. Res. Lett.* 45 (18), 9710–9720. <https://doi.org/10.1029/2018gl079419>.

- Davis, N.F.G., Mathews, W.H., 1944. Four phases of glaciation with illustrations from southwestern British Columbia. *J. Geol.* 52, 403–413. <https://www.jstor.org/stable/30068305>.
- Davis, P.T., Briner, J.P., Coulthard, R.D., Finkel, R.W., Miller, G.H., 2006. Preservation of Arctic landscapes overridden by cold-based ice sheets. *Quat. Res.* 65 (1), 156–163. <https://doi.org/10.1016/j.yqres.2005.08.019>.
- Duffer, H.E., Margold, M., 2021. Glacial geomorphology of the central sector of the Cordilleran ice sheet, northern British Columbia, Canada. *J. Maps* 17 (2), 413–427. <https://doi.org/10.1080/17445647.2021.1937729>.
- Duffer, H.E., Margold, M., Engel, Z., Braucher, R., the Aster Team, 2021. Using  $^{10}\text{Be}$  dating to determine when the Cordilleran ice sheet stopped flowing over the Canadian Rocky mountains. *Quat. Res.* 102, 222–233. <https://doi.org/10.1017/qua.2020.122>.
- Dyke, A.S., 1993. Landscapes of cold-centered late Wisconsinan ice caps, Arctic Canada. *Prog. Phys. Geogr.: Earth Environ.* 17 (2), 223–247. <https://doi.org/10.1177/030913339301700208>.
- Dyke, A.S., 2004. An outline of North American deglaciation with emphasis on central and northern Canada. In: Ehlers, J., Gibbard, P.L. (Eds.), *Developments in Quaternary Sciences*, vol. 2. Elsevier, pp. 373–424. [https://doi.org/10.1016/S1571-0866\(04\)80209-4](https://doi.org/10.1016/S1571-0866(04)80209-4).
- Engstrom, D.R., Hansen, B.C.S., Wright Jr., H.E., 1990. A possible Younger Dryas record in southeastern Alaska. *Science* 250, 1383–1385. <https://doi.org/10.1126/science.250.4986.1383>.
- Fabel, D., Fink, D., Harbor, J., Land, M., Stroeven, A.P., 2006. Exposure ages from relict lateral moraines overridden by the Fennoscandian ice sheet. *Quat. Res.* 65 (1), 136–146. <https://doi.org/10.1016/j.yqres.2005.06.006>.
- Flint, R.F., 1943. Growth of north American ice sheet during the Wisconsin age. *GSA Bull.* 54 (3), 325–363. <https://doi.org/10.1130/GSAB-54-325>.
- Friele, P.A., Clague, J.J., 2002. Younger Dryas readvance in Squamish river valley, southern Coast mountains, British Columbia. *Quat. Sci. Rev.* 21 (18), 1925–1933. [https://doi.org/10.1016/S0277-3791\(02\)00081-1](https://doi.org/10.1016/S0277-3791(02)00081-1).
- Fulton, R., 1971. Radiocarbon geochronology of southern British Columbia. *Geological Survey of Canada paper* 71-37, 28. <https://doi.org/10.4095/102467>.
- Fulton, R., 1991. A conceptual model for growth and decay of the Cordilleran ice sheet. *Geogr. Phys. Quaternaire* 45 (3), 281–286. <https://doi.org/10.7202/032875ar>.
- Gabrielse, H., 1963. McDame Map Area, Cassiar District, British Columbia. *Geological Survey of Canada*. <https://doi.org/10.4095/100546>. Memoir 319.
- Gabrielse, H., 1988. Geology of the Cry Lake and Dease Lake Map Areas, North-Central British Columbia. *Geological Survey of Canada*. <https://doi.org/10.4095/210074>. Bulletin 504.
- German Aerospace Center, 2018. TanDEM-X – Digital Elevation Model (DEM) – Global, 12 M. <https://gdk.gdi-de.org/geonetwork/srv/api/records/5eedcf4c-de57-4624-99e9-60086b032aea>. (Accessed 15 January 2020).
- Glasser, P.F., Bennett, R., 2004. Glacial erosion landforms: origins and significance for paleogeology. *Proc. Phys. Geogr.* 28 (1), 43–75. <https://doi.org/10.1191/0309133304pp401ra>.
- Gosse, J.C., Phillips, F.M., 2001. Terrestrial in situ cosmogenic nuclides: theory and application. *Quat. Sci. Rev.* 20 (14), 1475–1560. [https://doi.org/10.1016/S0277-3791\(00\)00171-2](https://doi.org/10.1016/S0277-3791(00)00171-2).
- Greenwood, S.L., Clark, C.D., 2009. Reconstructing the last Irish Ice Sheet 1: changing flow geometries and ice flow dynamics deciphered from the glacial landform record. *Quat. Sci. Rev.* 28 (27–28), 3085–3100. <https://doi.org/10.1016/j.yqres.2009.09.008>.
- Greenwood, S.L., Clark, C.D., Hughes, A.L.C., 2007. Formalising an inversion methodology for reconstructing ice-sheet retreat patterns from meltwater channels: application to the British Ice Sheet. *J. Quat. Sci.* 22 (6), 637–645. <https://doi.org/10.1002/jqs.1083>.
- Greenwood, S.L., Clason, C.C., Helanow, C., Margold, M., 2016. Theoretical, contemporary observational and palaeo-perspectives on ice sheet hydrology: processes and products. *Earth Sci. Rev.* 155, 1–27. <https://doi.org/10.1016/j.earscirev.2016.01.010>.
- Heaton, T.J., Köhler, P., Butzin, M., Bard, E., Reimer, R.W., Austin, W.E.N., Bronk Ramsey, C., Grootes, P.M., Hughen, K.A., Kromer, B., Reimer, P.J., Adkins, J., Burke, A., Cook, M.S., Olsen, J., Skinner, L.C., 2020. Marine20—the marine radiocarbon age calibration curve (0–55,000 cal BP). *Radiocarbon* 62 (4), 779–820. <https://doi.org/10.1017/rdc.2020.68>.
- Hebrand, M., Åmark, M., 1989. Esker formation and glacier dynamics in eastern Skane and adjacent areas, southern Sweden. *Boreas* 18 (1), 67–81. <https://doi.org/10.1111/j.1502-3885.1989.tb00372.x>.
- Hetherington, R., Reid, R.G.B., 2003. Malacological insights into the marine ecology and changing climate of the late Pleistocene-early Holocene Queen Charlotte Islands archipelago, western Canada, and implications for early people. *Can. J. Zool.* 81, 626–661. <https://doi.org/10.1139/z03-024>.
- Hewitt, I.J., Creyts, T.T., 2019. A model for the formation of eskers. *Geophys. Res. Lett.* 46 (12), 6673–6680. <https://doi.org/10.1029/2019GL082304>.
- Heyman, J., 2021. Expage. Retrieved 1 June 2021 from. <http://expage.github.io/index.html>.
- Hughes, A.L.C., Clark, C.D., Jordan, C.J., 2014. Flow-pattern evolution of the last British ice sheet. *Quat. Sci. Rev.* 89, 148–168. <https://doi.org/10.1016/j.yqres.2014.02.002>.
- Jackson, L., Ward, B., Duk-Rodkin, A., Hughes, O., 1991. The last Cordilleran ice sheet in southern Yukon territory. *Geogr. Phys. Quaternaire* 45 (3), 341–354. <https://doi.org/10.7202/032880ar>.
- Kennedy, K.E., Bond, J., 2004. Evidence for a late-McConnell readvance of the Cassiar Lobe in Seagull Creek, Pelly mountains, central Yukon. In: Emond, D.S., Lewis, L.L. (Eds.), *Yukon Exploration and Geology 2003*. Yukon Geological Survey, pp. 121–128.
- Kienast, S.S., McKay, J.L., 2001. Sea surface temperatures in the subarctic northeast Pacific reflect millennial-scale climate oscillations during the last 16 kyr. *Geophys. Res. Lett.* 28 (8), 1563–1566. <https://doi.org/10.1029/2000gl12543>.
- Kleman, J., Borgström, I., Robertsson, A.-M., Lilliesköld, M., 1992. Morphology and stratigraphy from several deglaciations in the Transtrand Mountains, western Sweden. *J. Quat. Sci.* 7 (1), 1–17. <https://doi.org/10.1002/jqs.3390070102>.
- Kleman, J., 1994. Preservation of landforms under ice sheets and ice caps. *Geomorphology* 9 (1), 19–32. [https://doi.org/10.1016/0169-555x\(94\)90028-0](https://doi.org/10.1016/0169-555x(94)90028-0).
- Kleman, J., Borgström, I., 1996. Reconstruction of paleo-ice sheets: the use of geomorphological data. *Earth Surf. Process. Landforms* 21 (10), 893–909. [https://doi.org/10.1002/\(SICI\)1096-9837\(199610\)21:10<893::AID-ESP620>3.0.CO;2-U](https://doi.org/10.1002/(SICI)1096-9837(199610)21:10<893::AID-ESP620>3.0.CO;2-U).
- Kleman, J., Hättestrand, C., Borgström, I., Stroeven, A., 1997. Fennoscandian palaeogeology reconstructed using a glacial geological inversion model. *J. Glaciol.* 43 (144), 283–299. <https://doi.org/10.3189/S0022143000003233>.
- Kleman, J., Hättestrand, C., Stroeven, A.P., Jansson, K.N., De Angelis, H., Borgström, I., 2006. Reconstruction of palaeo-ice sheets - inversion of their glacial geomorphological record. In: Knight, P.G. (Ed.), *Glacier Science and Environmental Change*. Blackwell Publishing Ltd. <https://doi.org/10.1002/9780470750636.ch38>.
- Kleman, J., Jansson, K., De Angelis, H., Stroeven, A.P., Hättestrand, C., Alm, G., Glasser, N., 2010. North American Ice Sheet build-up during the last glacial cycle, 115–21kyr. *Quat. Sci. Rev.* 29 (17–18), 2036–2051. <https://doi.org/10.1016/j.yqres.2010.04.021>.
- Kovane, D.J., 2002. Morphologic and stratigraphic evidence for Allerød and Younger Dryas age glacier fluctuations of the Cordilleran Ice Sheet, British Columbia, Canada and Northwest Washington, U.S.A. *Boreas* 31 (2), 163–184. <https://doi.org/10.1111/j.1502-3885.2002.tb01064.x>.
- Kovane, D.J., Easterbrook, D.J., 2002. Timing and extent of Allerød and Younger Dryas age (ca. 12,500–10,000 14C yr B.P.) oscillations of the Cordilleran Ice Sheet in the Fraser Lowland, western North America. *Quat. Res.* 57 (2), 208–224. <https://doi.org/10.1006/qres.2001.2307>.
- Lacourse, T., 2005. Late Quaternary dynamics of forest vegetation on northern Vancouver Island, British Columbia, Canada. *Quat. Sci. Rev.* 24, 105–121. <https://doi.org/10.1016/j.yqres.2004.05.008>.
- Lakeman, T.R., Clague, J.J., Menounos, B., 2008a. Advance of alpine glaciers during final retreat of the Cordilleran ice sheet in the Finlay River area, northern British Columbia, Canada. *Quat. Res.* 69 (2), 188–200. <https://doi.org/10.1016/j.yqres.2008.01.002>.
- Lakeman, T.R., Hollings, A.E., Clague, J.J., Menounos, B., Osborn, G.D., Jensen, B.J.L., Froese, D.G., 2008b. Holocene tephras in lake cores from northern British Columbia, Canada. *Can. J. Earth Sci.* 45 (8), 935–947. <https://doi.org/10.1139/e08-035>.
- Lambeck, K., Purcell, A., Zhao, S., 2017. The North American Late Wisconsin ice sheet and mantle viscosity from glacial rebound analyses. *Quat. Sci. Rev.* 158, 172–210. <https://doi.org/10.1016/j.yqres.2016.11.033>.
- Lane, T.P., Paasche, Ø., Kvisvik, B., Adamson, K.R., Rodés, Á., Patton, H., Gomez, N., Georghiu, D., Bakke, J., Hubbard, A., 2020. Elevation Changes of the Fennoscandian Ice Sheet Interior During the Last Deglaciation. *Geophys. Res. Lett.* 47 (14). <https://doi.org/10.1029/2020gl088796>.
- Lesnek, A.J., Briner, J.P., Baichtal, J.F., Lyles, A.S., 2020. New constraints on the last deglaciation of the Cordilleran Ice Sheet in coastal Southeast Alaska. *Quat. Res.* 96, 140–160. <https://doi.org/10.1017/qua.2020.32>.
- Lesnek, A.J., Briner, J.P., Lindqvist, C., Baichtal, J.F., Heaton, T.H., 2018. Deglaciation of the Pacific coastal corridor directly preceded the human colonization of the Americas. *Sci. Adv.* 4 (5). <https://doi.org/10.1126/sciadv.aar5040> eaar5040.
- Lifton, N., Sato, T., Dunai, T.J., 2014. Scaling in situ cosmogenic nuclide production rates using analytical approximation to atmospheric cosmic-ray fluxes. *Earth Planet. Sci. Lett.* 386, 149–160. <https://doi.org/10.1016/j.epsl.2013.10.052>.
- Livingstone, S.J., Storrar, R.D., Hillier, J.K., Stokes, C.R., Clark, C.D., Tarasov, L., 2015. An ice-sheet scale comparison of eskers with modelled subglacial drainage routes. *Geomorphology* 246, 104–112. <https://doi.org/10.1016/j.geomorph.2015.06.016>.
- Luckman, B.H., Osborn, G.D., 1979. Holocene glacier fluctuations in the middle Canadian Rocky Mountains. *Quat. Res.* 11 (1), 52–77. [https://doi.org/10.1016/0033-5894\(79\)90069-3](https://doi.org/10.1016/0033-5894(79)90069-3).
- Mangerud, J., Hughes, A.L.C., Sæle, T.H., Svendsen, J.I., 2019. Ice-flow patterns and precise timing of ice sheet retreat across a dissected fjord landscape in western Norway. *Quat. Sci. Rev.* 214, 139–163. <https://doi.org/10.1016/j.yqres.2019.04.032>.
- Mannerfelt, C.M., 1945. Några glacialmorfologiska förhållanden och deras vittnesbörd om inlandsisens avsmältningmekanik i svensk och norsk fjällterräng. *Geogr. Ann.* 27, 3–239. <https://doi.org/10.2307/520067>.
- Mannerfelt, C.M., 1949. Marginal drainage channels as indicators of the gradients of Quaternary ice caps. *Geogr. Ann.* 31, 194–199. <https://doi.org/10.2307/520362>.
- Marcott, S.A., Clark, P.U., Shakun, J.D., Brook, E.J., Davis, P.T., Caffee, M.W., 2019.  $^{10}\text{Be}$  age constraints on latest Pleistocene and Holocene cirque glaciation across the western United States. *npj Clim. Atmos. Sci.* 2 (1). <https://doi.org/10.1038/s41612-019-0062-z>.
- Margold, M., Gosse, J.C., Hidy, A.J., Woywitka, R.J., Young, J.M., Froese, D., 2019. Beryllium-10 dating of the Foothills Erratics Train in Alberta, Canada, indicates detachment of the Laurentide Ice Sheet from the Rocky Mountains at ~15 ka. *Quat. Res.* 92 (2), 469–482. <https://doi.org/10.1017/qua.2019.10>.

- Margold, M., Jansson, K.N., Kleman, J., Stroeven, A.P., 2013a. Lateglacial ice dynamics of the Cordilleran Ice Sheet in northern British Columbia and southern Yukon Territory: retreat pattern of the Liard Lobe reconstructed from the glacial landform record. *J. Quat. Sci.* 28 (2), 180–188. <https://doi.org/10.1002/jqs.2604>.
- Margold, M., Jansson, K.N., Kleman, J., Stroeven, A.P., Clague, J.J., 2013b. Retreat pattern of the Cordilleran Ice Sheet in central British Columbia at the end of the last glaciation reconstructed from glacial meltwater landforms. *Boreas* 42 (4), 830–847. <https://doi.org/10.1111/bor.12007>.
- Margold, M., Stokes, C.R., Clark, C.D., 2015. Ice streams in the Laurentide Ice Sheet: Identification, characteristics and comparison to modern ice sheets. *Earth Sci. Rev.* 143, 117–146. <https://doi.org/10.1016/j.earscirev.2015.01.011>.
- Margold, M., Stokes, C.R., Clark, C.D., 2018. Reconciling records of ice streaming and ice margin retreat to produce a palaeogeographic reconstruction of the deglaciation of the Laurentide Ice Sheet. *Quat. Sci. Rev.* 189, 1–30. <https://doi.org/10.1016/j.quascirev.2018.03.013>.
- Margold, M., Stroeven, A.P., Clague, J.J., Heyman, J., 2014. Timing of terminal Pleistocene deglaciation at high elevations in southern and central British Columbia constrained by  $^{10}\text{Be}$  exposure dating. *Quat. Sci. Rev.* 99, 193–202. <https://doi.org/10.1016/j.quascirev.2014.06.027>.
- Mathewes, R.W., 1993. Evidence for Younger Dryas-age cooling on the North Pacific coast of America. *Quat. Sci. Rev.* 12 (5), 321–331. [https://doi.org/10.1016/0277-3791\(93\)90040-s](https://doi.org/10.1016/0277-3791(93)90040-s).
- Mathewes, R.W., Heusser, L.E., Patterson, R.T., 1993. Evidence for a Younger Dryas-like event on the British Columbia coast. *Geology* 21, 101–104. [https://doi.org/10.1130/0091-7613\(1993\)021<0101:EFAYDL>2.3.CO;2](https://doi.org/10.1130/0091-7613(1993)021<0101:EFAYDL>2.3.CO;2).
- Menounos, B., Goehring, B.M., Osborn, G., Margold, M., Ward, B., Bond, J., Clarke, G.K.C., Clague, J.J., Lakeman, T., Koch, J., Caffee, M.W., Gosse, J., Stroeven, A.P., Seguinot, J., Heyman, J., 2017. Cordilleran Ice Sheet mass loss preceded climate reversals near the Pleistocene Termination. *Science* 358 (6364), 781–784. <https://doi.org/10.1126/science.aan3001>.
- Menounos, B., Osborn, G., Clague, J.J., Luckman, B.H., 2009. Latest Pleistocene and Holocene glacier fluctuations in western Canada. *Quat. Sci. Rev.* 28 (21–22), 2049–2074. <https://doi.org/10.1016/j.quascirev.2008.10.018>.
- Osborn, G., Gerloff, L., 1997. Latest pleistocene and early Holocene fluctuations of glaciers in the Canadian and northern American Rockies. *Quat. Int.* 38–39, 7–19. [https://doi.org/10.1016/S1040-6182\(96\)00026-2](https://doi.org/10.1016/S1040-6182(96)00026-2).
- Peltier, W.R., Argus, D.F., Drummond, R., 2015. Space geodesy constrains ice age terminal deglaciation: The global ICE-6G\_C (VM5a) model. *J. Geophys. Res. Solid Earth* 120 (1), 450–487. <https://doi.org/10.1002/2014JB011176>.
- Perkins, A.J., Brennand, T.A., 2015. Refining the pattern and style of Cordilleran Ice Sheet retreat: palaeogeography, evolution and implications of lateglacial ice-dammed lake systems on the southern Fraser Plateau, British Columbia, Canada. *Boreas* 44 (2), 319–342. <https://doi.org/10.1111/bor.12100>.
- Planet Team, 2017. Planet Application Program Interface: in Space for Life on Earth. <https://www.planet.com/markets/education-and-research/>.
- Plouffe, A., 2000. Quaternary geology of the Fort Fraser and Manson River map areas, central British Columbia. *Geol. Surv. Can. Bull.* 554. <https://doi.org/10.4095/211641>.
- Praetorius, S.K., Mix, A.C., 2014. Synchronization of North Pacific and Greenland climates preceded abrupt deglacial warming. *Science* 345 (6195), 444–448. <https://doi.org/10.1126/science.1252000>.
- Praetorius, S.K., Mix, A.C., Walczak, M.H., Wolhowe, M.D., Addison, J.A., Pahl, F.G., 2015. North Pacific deglacial hypoxic events linked to abrupt ocean warming. *Nature* 527 (7578), 362–366. <https://doi.org/10.1038/nature15753>.
- Rasmussen, S.O., Bigler, M., Blockley, S.P., Blunier, T., Buchardt, S.L., Clausen, H.B., Cvijanovic, I., Dahl-Jensen, D., Johnsen, S.J., Fischer, H., Gkinis, V., Guillevic, M., Hoek, W.Z., Lowe, J.J., Pedro, J.B., Popp, T., Seierstad, I.K., Steffensen, J.P., Svensson, A.M., Vallelonga, P., Vinther, B.M., Walker, M.J.C., Wheatley, J.J., Winstrup, M., 2014. A stratigraphic framework for abrupt climatic changes during the Last Glacial period based on three synchronized Greenland ice-core records: refining and extending the INTIMATE event stratigraphy. *Quat. Sci. Rev.* 106, 14–28. <https://doi.org/10.1016/j.quascirev.2014.09.007>.
- Reasoner, M.A., Osborn, G., Rutter, N.W., 1994. Age of the Crowfoot advance in the Canadian Rocky Mountains: A glacial event coeval with the Younger Dryas oscillation. *Geology* 22 (5). [https://doi.org/10.1130/0091-7613\(1994\)022<0439:Aotcai>2.3.CO;2](https://doi.org/10.1130/0091-7613(1994)022<0439:Aotcai>2.3.CO;2).
- Reimer, P.J., Austin, W.E.N., Bard, E., Bayliss, A., Blackwell, P.G., Bronk Ramsey, C., Butzin, M., Cheng, H., Edwards, R.L., Friedrich, M., Grootes, P.M., Guilderson, T.P., Hajdas, I., Heaton, T.J., Hogg, A.G., Hughen, K.A., Kromer, B., Manning, S.W., Muscheler, R., Palmer, J.G., Pearson, C., Van Der Plicht, J., Reimer, R.W., Richards, D.A., Scott, E.M., Southon, J.R., Turney, C.S.M., Wacker, L., Adolphi, F., Büntgen, U., Capano, M., Fahrni, S.M., Fogtmann-Schulz, A., Friedrich, R., Köhler, P., Kudsk, S., Miyake, F., Olsen, J., Reinig, F., Sakamoto, M., Sookdeo, A., Talamo, S., 2020. The IntCal20 Northern Hemisphere Radiocarbon Age Calibration Curve (0–55 cal kBP). *Radiocarbon* 62 (4), 725–757. <https://doi.org/10.1017/rdc.2020.41>.
- Ryder, J.M., 1989. Climate (Canadian Cordillera). In: Fulton, R.J. (Ed.), *Quaternary Geology of Canada and Greenland*, 26–31. Geological Survey of Canada, Geology of Canada 1, Ottawa, ON.
- Ryder, J.M., Maynard, D., 1991. The Cordilleran Ice Sheet in Northern British Columbia. *Geogr. Phys. Quaternaire* 45 (3), 355–363. <https://doi.org/10.7202/032881ar>.
- Sacco, D.A., Ward, B.C., Lian, O.B., Maynard, D.E., Geertsema, M., 2017. Quaternary geology of part of the McLeod Lake map area (NTS 093J), central British Columbia: lithostratigraphy, glacial history, and chronology. *Can. J. Earth Sci.* 54 (10), 1063–1084. <https://doi.org/10.1139/cjes-2016-0198>.
- Seguinot, J., 2020. *Cordilleran ice sheet glacial cycle simulations continuous variables* (Version 1). <https://doi.org/10.5281/zenodo.3606535>. (Accessed 5 October 2020).
- Seguinot, J., Rogozhina, I., Stroeven, A.P., Margold, M., Kleman, J., 2016. Numerical simulations of the Cordilleran ice sheet through the last glacial cycle. *Cryosphere* 10 (2), 639–664. <https://doi.org/10.5194/tc-10-639-2016>.
- Shaw, J., Sharpe, D., Harris, J., 2010. A flowline map of glaciated Canada based on remote sensing data. *Can. J. Earth Sci.* 47 (1), 89–101. <https://doi.org/10.1139/E09-068>.
- Shaw, J., Stacey, C.D., Wu, Y., Lintern, D.G., 2017. Anatomy of the Kitimat fiord system, British Columbia. *Geomorphology* 293, 108–129. <https://doi.org/10.1016/j.geomorph.2017.04.043>.
- Shulmeister, J., Fink, D., Winkler, S., Thackray, G.D., Borsellino, R., Hemmingsen, M., Rittenour, T.M., 2018. Evidence for slow late-glacial ice retreat in the upper Rangitata Valley, South Island, New Zealand. *Quat. Sci. Rev.* 185, 102–112. <https://doi.org/10.1016/j.quascirev.2018.01.006>.
- Spooner, I.S., Osborn, G.D., 2000. Geomorphology and Late Wisconsinian sedimentation in the Stikine River Valley, northern British Columbia. *Quat. Int.* 68–71, 285–296. [https://doi.org/10.1016/S1040-6182\(00\)00051-3](https://doi.org/10.1016/S1040-6182(00)00051-3).
- Stokes, C.R., Clark, C.D., 1999. Geomorphological criteria for identifying Pleistocene ice streams. *Ann. Glaciol.* 28, 67–74. <https://doi.org/10.3189/172756499781821625>.
- Stokes, C.R., Tarasov, L., Blomdin, R., Cronin, T.M., Fisher, T.G., Gyllencreutz, R., Hättestrand, C., Heyman, J., Hindmarsh, R.C.A., Hughes, A.L.C., Jakobsson, M., Kirchner, N., Livingstone, S.J., Margold, M., Murton, J.B., Noormets, R., Peltier, W.R., Peteet, D.M., Piper, D.J.W., Preusser, F., Renssen, H., Roberts, D.H., Roche, D.M., Saint-Angé, F., Stroeven, A.P., Teller, J.T., 2015. On the reconstruction of palaeo-ice sheets: Recent advances and future challenges. *Quat. Sci. Rev.* 125, 15–49. <https://doi.org/10.1016/j.quascirev.2015.07.016>.
- Stroeven, A.P., Hättestrand, C., Kleman, J., Heyman, J., Fabel, D., Fredin, O., Goodfellow, B.W., Harbor, J.M., Jansen, J.D., Olsen, L., Caffee, M.W., Fink, D., Lundqvist, J., Rosqvist, G.C., Strömberg, B., Jansson, K.N., 2016. Deglaciation of Fennoscandia. *Quat. Sci. Rev.* 147, 91–121. <https://doi.org/10.1016/j.quascirev.2015.09.016>.
- Stuiver, M., Reimer, P.J., 1993. Extended  $^{14}\text{C}$  data base and revised CALIB 3.0  $^{14}\text{C}$  age calibration program. *Radiocarbon* 35, 215–230. <https://doi.org/10.1017/S003822200013904>.
- Stumpf, A.J., Broster, B.E., Levson, V.M., 2000. Multiphase flow of the late Wisconsinian Cordilleran ice sheet in Western Canada. *Geol. Soc. Am. Bull.* 112 (12), 1850–1863. <http://pubs.er.usgs.gov/publication/70022374>.
- Syverson, K.M., Mickelson, D.M., 2009. Origin and significance of lateral meltwater channels formed along a temperate glacier margin, Glacier Bay, Alaska. *Boreas* 38 (1), 132–145. <https://doi.org/10.1111/j.1502-3885.2008.00042.x>.
- Taylor, M.A., Hendy, I.L., Pak, D.K., 2014. Deglacial ocean warming and marine margin retreat of the Cordilleran Ice Sheet in the North Pacific Ocean. *Earth Planet Sci. Lett.* 403, 89–98. <https://doi.org/10.1016/j.epsl.2014.06.026>.
- Turner, D.G., Ward, B., Bond, J., 2008. Glacial history of Howard's Pass and applications to drift prospecting. In: Emond, D.S., Blackburn, L.R., Hill, R.P., Weston, L.H. (Eds.), *Yukon Exploration and Geology 2007*. Yukon Geological Survey, pp. 257–272.
- Vionnet, V., Mortimer, C., Brady, M., Arnal, L., Brown, R., 2021. Canadian historical Snow Water Equivalent dataset (CanSWE, 1928–2020). *Earth Syst. Sci. Data* 13 (9), 4603–4619. <https://doi.org/10.5194/essd-13-4603-2021>.
- Walczak, M.H., Mix, A.C., Cowan, E.A., Fallon, S., Fifield, L.K., Alder, J.R., Du, J., Haley, B., Hobern, T., Padman, J., Praetorius, S.K., Schmittner, A., Stoner, J.S., Zellers, S.D., 2020. Phasing of millennial-scale climate variability in the Pacific and Atlantic oceans. *Science* 360 (6517), 716–720. <https://doi.org/10.1126/science.aba7096>.
- Watson, K., Mathews, W.H., 1944. *The Tuya-Teslin Area, Northern British Columbia*, vol. 19. British Columbia Department of Mines, Bulletin.
- Young, N.E., Briner, J.P., Schaefer, J., Zimmerman, S., Finkel, R.C., 2019. Early Younger Dryas glacier culmination in southern Alaska: Implications for North Atlantic climate change during the last deglaciation. *Geology* 47 (6), 550–554. <https://doi.org/10.1130/g46058.1>.